TITLE PAGE

An overview of in situ digital photographic approaches to estimate forest canopy attributes

Francesco CHIANUCCI[1,*]

[1] CREA– Research Centre for Forestry and Wood, viale S. Margherita 80, Arezzo (Italy)

[*]Corresponding author (fchianucci@gmail.com; francesco.chianucci@crea.gov.it)

Abstract

Since the 1960s, canopy photography has been widely used in forestry. Hemispherical photography was once the most widely used technique, but its widespread adoption was limited by the time-consuming nature of image processing and the sensitivity of the results to hemispherical image acquisition and processing.

Over the last decade, a number of alternative restricted view angle photographic approaches have been proposed. Cover photography acquired via a normal lens was the first of the recently introduced photographic techniques. Use of a restricted view, often fixed lens has subsequently contributed to the extension of canopy photography to new sensors and platforms, which ultimately have provided answers to some previous challenges, regarding within-crown clumping correction, isolated and urban tree measurements, understory assessment, operational leaf inclination angle measurements, and phenological monitoring.

The study provides a comprehensive review of the use of canopy photography in forestry and describes the theory and definitions of the variables used to quantify canopy structure. A case study is presented to illustrate and compare the different features and performance of the existing overstory photographic techniques; results make it possible to suggest sampling strategies for consistent overstory canopy photographic measurements. Emerging operational fields of canopy photography are also described and discussed.

Keywords: canopy photography; leaf area index; restricted view angle sensors; hemispherical sensors; canopy cover; canopy openness

1. Introduction

Accurate *in situ* measurements of forest canopy are essential for a wide range of studies. As the canopy is more sensitive and reacts more promptly than other stand components to disturbances, field measurements of canopy structure are also widely used for establishing forest research and monitoring programs (e.g., Baret et al. 2008; Fleck et al. 2016). As the canopy affects vegetation reflectance from optical satellite imagery (Dawson et al. 1999; Kuusk et al. 2013; Weiss et al. 2004), field estimates of canopy structure are also used for validating remotely sensed information (Baret et al. 2008).

Leaf area index (LAI), defined as half the total leaf area per horizontal ground area (Chen and Black 1992), is one of the most commonly used canopy attributes. In forest stands, LAI is routinely estimated using indirect optical methods owing to the disadvantages of direct methods, which are time-consuming, labour intensive and often destructive. Canopy photography is a widely used indirect method for estimating LAI and other forest canopy attributes. Film hemispherical photography (FHP) was the first photographic technique used in forestry. Evans and Coombe (1959) first used the fisheye lens developed by Hill (1924) to analyse light penetration under the forest canopy using FHP. This photographic technique was then widely used to estimate forest canopy attributes (Anderson 1964, 1971, 1981, Bonhomme et al. 1972, Chan et al. 1986, Wang and Miller 1987). However, technical and theoretical drawbacks have progressively hindered widespread adoption of FHP (Bréda 2003, Chianucci and Cutini 2012). The advances observed in digital photographic technology in the last two decades, combined with the low prices of cameras and lenses, the development of various tools and software for processing hemispherical images (Diaz and Lencinas 2015; Macfarlane 2011), and advances in digital raw image processing (Hwang et al. 2016; Lang et al. 2017; Macfarlane et al. 2014), have led to an increasing interest in the use of digital hemispherical photography (DHP) to estimate forest canopy attributes.

Notwithstanding these improvements, a great drawback in DHP is that measurements of gap fraction, from which estimates of LAI are derived, are sensitive to camera exposure (Macfarlane 2000; Zhang et al. 2005), image processing (Jonckheere et al. 2004; Leblanc et al. 2005; Wagner and Hagemeier, 2006) and gamma correction (Macfarlane et al. 2007c), which severely hinders comparisons because of a lack of standard protocols for acquisition and analysis of hemispherical images (Beckschäfer et al. 2013).

As an alternative to hemispherical photography, restricted view photography (RVP) has been developed for estimating LAI. A first RVP approach, which was based on images taken at 57°, was proposed by Bonhomme and Chartier (1972). The rationale behind this approach is that gap fraction measurements at 1 radian (~57.3°) are insensitive to leaf inclination angle, making the LAI estimation independent of the orientation of the leaves.

Alternative RVP approaches have been introduced for canopy analysis in the last decade. Digital cover photography (DCP) was among the first of the recently introduced RVP approaches (Macfarlane et al. 2007a,b,c). DCP images are acquired using a normal lens (i.e., a lens with a focal length approximately equal to the diagonal of the film format of a digital camera's image sensor) oriented upward (i.e., at the zenith). The resulting narrow field of view (FOV) maximizes the full frame, which brings several advantages, such as higher sampling

resolution close to the zenith (all the image pixels are used to sample this portion of the canopy) and lower sensitivity to camera exposure. The main limitation of DCP is that it requires independent measurements of leaf inclination angle to estimate LAI from gap fraction. However, this limitation has recently been overcome by introducing either new photographic approaches (Ryu et al. 2010) or new technical photographic procedures (Piayda et al. 2015).

The use of RVPs has favoured the extension of digital photography to new operational fields such as understory and urban tree assessment, but most of these applications in forestry are still at an experimental stage.

This study provides an overview of established (i.e., DHP and 57°) and recently developed canopy photographic approaches. A case study is presented to illustrate sampling strategies for consistent photographic measurement of the overstory. Recent and emerging forest canopy applications using RVP are also illustrated and discussed.

2. Basic theory and definitions

Indirect optical methods such as canopy photography infer LAI and other canopy attributes from measurements of radiation transmission through the canopy, making use of radiative transfer theory (Ross 1981). These non-destructive methods are based on a probabilistic approach to foliar element ratio (or its complement, gap fraction), distribution and arrangement within the canopy (Monsi and Saeki 1953). LAI is calculated by inversion of the Beer-Lambert law, which computes gap fraction as (Equation 1):

$$P(\theta) = \exp\left(-\frac{G(\theta)LAI}{cos\ \theta} \right) \quad (1)$$

Here $P(\theta)$ is the gap fraction at a given zenith angle θ. $G(\theta)$ is the G-function and corresponds to the fraction of foliage projected on the plane normal to the θ direction. G-function depends on θ and the leaf inclination angle (θ_L). Equation 1 assumes a random distribution of foliage, which rarely occurs in real canopies. For this reason, a clumping index $\Omega(\theta)$ is introduced in Equation (1) and its inversion (Equation 2, after Nilson 1971):

$$P(\theta) = \exp\left(-\frac{G(\theta)\Omega(\theta)LAI}{cos\theta} \right) \quad (2)$$

Here $\Omega(\theta)$ is dependent on the zenith angle θ. The product of the clumping index and LAI is called the effective leaf area index (LAI_e), which ignores clumping; the true LAI is the leaf area index corrected for clumping. To avoid variation with θ, a mean clumping index, Ω, is often calculated as the ratio of LAI_e to true LAI (Chen et al. 1997; Leblanc et al. 2005). Ω is calculated from gap fraction by analysis of gap size distribution (Chen and Cihlar 1995) or analysis of the gap fraction distribution of a number of azimuth segments for each annulus (zenith ring) of the hemisphere (Lang and Xiang 1986, Van Gardingen et al. 1999). Alternatively, combined approaches proposed by Leblanc (2002) and Chianucci et al. (2019) can also be used. These clumping correction formulae are reported in Table 1.

[TABLE 1]

The G-function is related to θ_L and the leaf angle distribution function $f(\theta_L)$. Assuming an azimuthally symmetric canopy, the formula is (Warren Wilson 1960):

$$G(\theta) = \int_0^{\pi/2} A(\theta,\theta_L) f(\theta_L) d\theta_L \quad (3)$$

where A is the projection coefficient at a given θ_L and θ (Warren Wilson 1960):

$$A(\theta,\theta_L) = \begin{cases} cos\theta cos\theta_L & |cot\theta cot\theta_L| > 1 \\ cos\theta cos\theta_L[1 + (2/\pi)(\tan\psi - \psi)] & |cot\theta cot\theta_L| \leq 1 \end{cases} \quad (4)$$

$$\psi = cos^{-1}(cot\theta cot\theta_L)$$

The ratio of $G(\theta)$ and $cos\theta$ in Equations 1 and 2 is often referred to as an extinction coefficient $k(\theta)$. The $f(\theta_L)$ can be more easily interpreted using six modelled distributions as determined from various authors (de Wit 1965; Goel and Strebel 1984; Goudriaan 1988; Ross 1981), based on empirical and mathematical considerations on leaf normal distribution (Figure 1 and Table 2). In spherical canopies, the relative frequency of leaf inclination angles is the same as that observed for the surface elements of a sphere. For uniform canopies, the frequency of leaf inclination angles is the same as that observed at any angle. Planophile canopies are

dominated by horizontal leaves. Plagiophile canopies are dominated by oblique leaves. Erectophile canopies are dominated by vertical leaves. Extremophile canopies show high frequencies of both horizontally and vertically oriented leaves. Summary statistics on these six distributions have been calculated by Goel and Strebel (1984) and are reported in Table 2. Although these distributions describe classical trends in the orientation of leaves, recent studies have demonstrated that the most frequent distributions in temperate and boreal forests are planophile, followed by plagiophile (Chianucci et al. 2018; Pisek et al. 2013), while the spherical distribution rarely occurs in these forests. No extremophile distribution was observed in the above-cited studies.

[FIGURE 1]

[TABLE 2]

In addition to LAI, canopy cover (CCO) is another commonly used variable in forestry (Angelini et al. 2015; Jennings et al. 1999) as well as in land-use/land-cover (LULC) studies. CCO can be defined as the average proportion of ground surface covered by the vertical projection of tree crowns (Jennings et al. 1999). If this definition includes within-crown gaps as part of the canopy, it is equivalent to the definition of crown cover proposed by Macfarlane et al. (2007b, c). CCO is generally estimated from indirect optical methods as the complement of gap fraction measured at a restricted view (generally at 0°-15° zenith angle range, which corresponds to the inner ring of LAI-2200; Rautiainen and Stenberg 2005; Chianucci 2016). In canopy photography, the formula for calculating CCO is:

$$CCO = 1 - \frac{N_L}{N_T} \quad (5)$$

where N_T is the total number of pixels and N_L is the total number of pixels located in the large gaps at the considered restricted view (0°-15°).

Conversely, Macfarlane et al. (2007b,c) define foliage cover (FCO) as the complement of total gap fraction (including within-crown and between-crowns gaps):

$$FCO = 1 - GF \quad (6)$$

where GF is the total gap fraction at the considered restricted view (0°-15°).

Canopy closure (CCL) is another variable commonly used in forestry (Gonsamo et al. 2013; Jennings et al. 1999; Paletto and Tosi 2009). CCL can be defined as the proportion of the entire sky hemisphere that is obstructed by vegetation when viewed from a single point. Based on this definition, CCL can be estimated as the complement of total gap fraction estimated from a hemispherical view sensor, weighted or not according to zenith angle.

3. Photographic approaches for estimating overstory canopy structure

For simplicity, passive optical methods can be divided into two main categories according to the sensor lenses used: the first group uses instruments with hemispherical view lenses, while the second group uses instruments with restricted view lenses.

3.1 Optical instruments with hemispherical view

The way to measure the largest footprint of a canopy in a single measurement is to use a sensor equipped with a fisheye lens. The sensor can be a camera (as in DHP) or a light sensor such as the one used in the LAI-2200 (which replaced the former LAI-2000 instrument) Plant Canopy Analyzer (LI-COR Inc., Nebraska, US; Figure 2). As the two instruments have similar theoretical background, the LAI-2200 is introduced briefly and compared with DHP below.

[FIGURE 2]

The LAI-2200 relies on the assumption that canopy elements are opaque and randomly distributed. Its FOV is limited to 0° - 74° zenith angle range, which is sampled across five concentric rings, each about 15° in size (Figure 2). The LAI-2200 measures light filtered in the 320-490 nm wavelength (blue) range, since leaves are nearly opaque at this range. Gap fraction is calculated from the LAI-2200 as the ratio of below-canopy measurements to simultaneous measurements obtained above the canopy (e.g., from an adjacent clearing or a tower). A major advantage of using a fisheye lens is that it allows estimation of LAI from Equation 1 without the need to parametrize G-function. Indeed, Miller (1967) noted that integrating G-function over the full zenith angle range gave:

$$\int_0^{\pi/2} G(\theta)\sin\theta d\theta = 0.5 \quad (7)$$

Hence, the inversion of Equation 1 in optical instruments with a hemispherical view is:

$$LAI = 2\int_0^{\pi/2} -lnP(\theta)cos\theta\ sin\theta\ d\theta \quad (8)$$

More specifically, considering that measurements with the LAI-2200 are performed at discrete zenith angle rings, the inversion of Equation 1 yields:

$$\text{LAI} = 2\sum_{i=1}^{n} -lnP(\theta_i)cos\theta_i\, w_i \quad (9)$$

where n=5 is the number of discrete zenith angles (zenith rings) of LAI-2200, θ_i denotes the i-th zenith ring, and w_i is the weighting factor, which is proportional to $sin\theta_i d\theta_i$ and normalized to sum to 1.0 (Welles and Norman 1991).

When multiple readings are available, Equation 7 can be computed in two ways:

$$\text{LAI}_e = 2\sum_{i=1}^{n} -ln\overline{P(\theta_i)}cos\theta_i\, w_i \quad (10a)$$

$$\text{LAI} = 2\sum_{i=1}^{n} -\overline{lnP(\theta_i)}cos\theta_i\, w_i \quad (10b)$$

LAI-2200 calculates an apparent clumping index, Ω_{APP}, as the ratio of the LAI_e calculated from Equation 10a to the LAI calculated from Equation 10b, and therefore it considers larger-scale clumping effects (the so-called apparent clumping index; Ryu et al. 2010).

Compared to the LAI-2200, DHP does not require above-canopy reference measurements. The hemispherical image is binarized (black and white), and gap fraction is then computed as the ratio of sky pixels over total image pixels. The blue channel is usually used for image analysis to address the assumption of opaque leaves. The advantage of DHP over LAI-2200 is that the hemispherical image can be divided into the desired number of zenith rings and azimuth segments, allowing a finer sampling of clumping according to the azimuth segment size considered (Chianucci et al. 2015a). Many other clumping corrections are also available in DHP. Table 3 summarizes the main differences between the two types of instrument.

The main disadvantage of canopy photography (including DHP) over other optical methods such as those using LAI-2200 is that data acquisition and processing are more difficult, as the

reliability of photographic methods is strongly affected by camera exposure, which is partly related to not using above-canopy reference measurements of current background light conditions. The major factors affecting the accuracy of canopy photography are illustrated in Paragraph 3.4.

[TABLE 3]

3.2 Restricted view photographic methods

RVP has the strong advantage that all the image pixels are used to sample specific important zenith regions such as the zenith (DCP) or the so-called hinge angle (57° photography). Another RVP technique based on images taken perpendicular to the tree canopy is used to measure the leaf inclination angle distribution of canopy foliage (levelled photography, LP).

3.2.1 Digital cover photography

DCP is a zenith observation method which is based on photographs acquired through a 70 mm equivalent focal-length lens (in 35 mm format) to obtain an approximately 30° FOV. From Figure 3, it can be seen that large between-crowns gaps can be easily resolved from DCP, particularly in sparse to medium-dense canopies. The separation between large and total gaps makes it possible to estimate two distinct canopy cover attributes (CCO and FCO) as previously described (see Equation 5-6; Macfarlane et al. 2007b,c).

Crown porosity (CP) is also calculated as the proportion of gaps within crown envelopes, excluding between-crowns gaps (Equation 11).

$$CP = 1 - \frac{FCO}{CCO} \quad (11)$$

The clumping index Ω_0 is calculated as (Equation 12):

$$\Omega_0 = \frac{(1 - CP) ln(1 - FCO)}{ln(CP)\mathrm{FCO}} \quad (12)$$

Another advantage related to DCP is the lower frequency of mixed pixels (those containing a portion of sky and canopy) compared with wide-angle photographic methods, which reduces the uncertainty of pixel classification (Chianucci 2016). In addition, sky luminance is more uniform, and therefore DCP is less sensitive to photographic exposure and gamma correction than DHP (Macfarlane et al. 2007b,c).

[FIGURE 3]

While FCO is directly retrieved, CCO and CP require the classification of large between-crowns gaps from total gap fraction using this photographic method. A very simple, albeit manual method (Chianucci and Cutini 2013) for classifying large gaps is based on the freeware GIMP (GNU image manipulation program; the GIMP team 2018). Using this software, large between-crowns gaps are selected using the 'fuzzy' tool, and the total number of relative pixels is recorded from the histogram. All gaps can then be selected using the 'select by color' tool, and the relative number of pixels within each gap recorded from the histogram. From the number of image pixels, large gap pixels, and total gap pixels, it is possible to estimate FCO, CCO and CP. Alternatively, an objective procedure for classifying large gaps has been proposed by Alivernini et al. (2018), based on the statistical distribution of gap sizes. The procedure has been implemented in the freely available software "CanopyCover" (CaCo; see Alivernini et al. 2018) and is insensitive to canopy density. Macfarlane et al. (2007b,c) proposed an alternative procedure based on gap area, where large gaps are identified as those larger than 1.3% of the image area.

Once CCO, FCP and CP are estimated from DCP, it is possible to calculate LAI, either with correction for clumping (LAI; Equation 13) or without correction (LAI_e; Equation 14).

$$LAI = -CCO\frac{\ln(CP)}{k} \quad (13)$$

$$LAI_e = -\frac{\ln(1-FCO)}{k} \quad (14)$$

Knowledge of the extinction coefficient k is required for LAI inversion using DCP. This

parameter can be measured using the LP method.

3.2.2 Fifty-seven degree (57°) photography

The 57° photographic method (Figure 4) was derived from the inclined point quadrat theory (Warren Wilson 1960), which demonstrated that the G-function converges to 0.5 (k=0.91) at 57°, irrespective of the leaf inclination angle distribution type (see Figure 1). The method has been shown to be comparable with DHP (Leblanc and Fournier 2014) when estimating LAI. The method can be derived from either RVP images oriented at 57° (Macfarlane et al. 2007c) or DHP images (Chianucci et al. 2019; Leblanc and Fournier 2014). However, it has some shortcomings:

- Few image pixels are used (when the method is derived from DHP), and only a limited portion of the canopy is sampled.
- The different FOV makes comparability with other methods difficult.
- The woody area index (WAI) increases with zenith angle (Kucharik et al. 1998), and thus LAI is underestimated if no corrections for woody area are performed.

[FIGURE 4]

3.2.3 Levelled photography

In the LP method proposed by Ryu et al. (2010), levelled images are acquired along the vertical canopy profile. Images can be collected using towers, extendable poles, ladders, nearby tall buildings or drones (UAVs; McNeil et al. 2016). Images can either be classified according to different canopy height levels (Raabe et al. 2015) or considered representative of the whole sampled tree canopy (Chianucci et al. 2018b; Pisek et al. 2013).

Once collected, the images are visually checked to identify the leaves suitable for photographic measurements of leaf inclination angle, i.e., those perpendicular to the camera's viewing direction (i.e., the leaves shown as a line in Figure 5). A previous study suggested a minimum sample size of 75 leaf angles per tree species (Pisek et al. 2013).

[FIGURE 5]

For each species, some leaf inclination angles (θ_L) can be measured using image software such as ImageJ (Schneider et al. 2012), assuming an isotropic azimuth distribution of foliage. Although the measurements are manually performed, the LP method is robust in terms of user sensitivity (Raabe et al. 2015) and improves the feasibility of measuring tall trees (Yan et al. 2019).

Once the θ_L are measured, their probability density can then be fitted using the two-parameter beta distribution, which has been shown to properly describe $f(\theta_L)$ (Goel and Strebel 1984; Campbell and Norman 1989) (Equation 15):

$$f(t) = \frac{1}{B(\mu,\nu)}(1-t)^{\mu-1}t^{\nu-1} \quad (15)$$

where $t=2\ \theta_L/\pi$ and θ_L is expressed in radians. The beta distribution, $B(\mu,\nu)$, is defined as (Equation 16):

$$B(\mu,\nu) = \int_0^1 (1-x)^{\mu-1}x^{\nu-1}dx = \frac{\Gamma(\mu)\Gamma(\nu)}{\Gamma(\mu+\nu)} \quad (16)$$

where Γ is the gamma function and μ and ν are the two parameters of the beta distribution, calculated as follows:

$$\mu = (1-\bar{t})\cdot\left(\frac{\sigma_0^2}{\sigma_t^2}-1\right) \quad (17)$$

$$\nu = \bar{t}\cdot\left(\frac{\sigma_0^2}{\sigma_t^2}-1\right) \quad (18)$$

where σ_0^2 is the maximum standard deviation with expected mean $\bar{t}$, and σ_t^2 is the variance of t (Wang et al. 2007).

Once a sufficient number of θ_L measurements have been taken, the *G*-function can be computed from θ_L and $f(\theta_L)$. A routine written in R (R Core Development Team) to calculate *G*-function from θ_L is freely available in Chianucci et al. (2017), along with a database of measured leaf inclination angles and distribution for 138 temperate and boreal woody species.

3.4 Factors affecting the accuracy of digital canopy photography

(1) Measurements with passive optical sensors are generally taken either at sunset or dusk under diffuse light conditions, or alternatively under a uniformly overcast sky. Under such conditions, light is dominated by the blue portion of the visible electromagnetic spectrum, where the foliage elements have much lower reflectivity and transmittance, making the foliage darker than in the other visible bands. In digital canopy photography, this procedure allows the best contrast between sky and non-sky pixels, facilitating image classification. By contrast, direct light conditions can threaten image classification by causing some artefacts in the images (e.g., blown highlights, flares, reflections; see also: Andis 2018). While LAI-2200 has introduced a procedure for estimating gap fraction under direct light conditions (see Kobayashi et al. 2013), avoidance of direct light is still recommended for acquisition of canopy images. Moving clouds should also be avoided, as they can cause blooming and quickly changing light conditions during measurements (Leblanc et al. 2005).

(2) Camera exposure affects the magnitude of the canopy gap fraction (Zhang et al. 2005). Automatic exposure is unable to yield reliable estimates of the gap fraction (Chen et al. 1991; Macfarlane et al. 2000; Zhang et al. 2005), causing underestimates in sparser canopies and overestimates in denser ones (Zhang et al. 2005). This issue is particularly relevant for DHP, considering the rather complex light distribution across its largest view (Yan et al. 2019). DCP is less affected by camera exposure (Chianucci and Cutini 2013; Macfarlane et al. 2007c). The desired exposure for canopy photography would be the one that makes the best contrast between canopy and sky pixels, with minimal saturation at either end of the brightness histogram (Leblanc et al. 2005).

A previous study (Beckschäfer et al. 2013) indicated that at least ten different approaches have been used to address the problem of photographic exposure in DHP, which limits the comparability among measurements obtained using different exposure protocols. Despite the efforts to address this issue from existing protocols (Fleck et al. 2016; ICOS 2014), the

standardization of the camera exposure procedure still represents a major issue in canopy photography, particularly in DHP.

As an alternative to setting the exposure, the use of raw image format can partly overcome the issue of determining the optimal camera exposure. The raw format contains the native scene captured by the camera sensor with minimally processed data, which needs to be converted into a viewable image format. The advantage is that shooting in raw mode makes it possible to capture the native scene's brightness at higher radiometric resolution (bit depth), which should *a-posteriori* be converted to the 8-bit range of a JPEG file, while simultaneously maximizing contrast (Macfarlane et al. 2014). Some studies (Macfarlane et al. 2014; Hwang et al. 2016) have indicated that this procedure has the potential to largely eliminate the influence of photographic exposure.

(3) Unlike film cameras, image sensors in digital cameras have the advantage of responding linearly to light (Zhang et al. 2005). However, to simulate the non-linear behavior of the human eye, the in-camera software applies a logarithmic transformation by means of a gamma function (Cescatti 2007). The gamma function describes the relation between actual light intensity during photography and the resulting brightness value of the pixel. A gamma value of 1.0 denotes an image that accurately reproduces actual light intensity. Digital cameras typically have gamma values between 2.0 and 2.5. The main effect of this correction is to lighten the mid-tones, which results in a biased estimate of canopy light transmittance (Cescatti 2007). Gamma function has more impact on DHP than on DCP (Macfarlane et al. 2007b,c). An advantage of shooting in raw mode is that the user has control of the gamma function that is applied to the raw data.

(4) The optimal light intensity (brightness value) from a color channel or grey-level image is used as the threshold value to distinguish pixels belonging to the sky or canopy, to produce a binary image (Jonckheere et al. 2004, Jonckheere et al. 2005, Cescatti 2007). Many binarization algorithms have been tested, including single thresholding methods (e.g., Otsu, Ridler-Calvard) or dual thresholding methods (e.g., the two-corner method - for a more complete description, see Macfarlane 2011; Glatthorn and Beckschäfer 2014).

In general, automatic thresholding methods should be preferred over manual methods, because of the subjectivity of the latter. Several automatic thresholding methods are available from freeware such as ImageJ or free programming language such as R. For example, the 'Auto Threshold' plugin (Landini et al. 2017) of ImageJ contains several automatic thresholding methods, which have been also translated in R within the 'authothresholdr' library (Nolan et al. 2019).

Image classification is closely related to camera exposure; indeed, previous studies (Grotti et al. 2020; Macfarlane 2011; Macfarlane et al. 2014) concluded that classification is of little importance if canopy and sky regions are well contrasted; therefore, shooting in raw mode and contrast-stretching the images can be an effective option for facilitating image classification while simultaneously minimizing the influence of camera exposure (Macfarlane et al. 2014). Table 4 lists the main features of some available DHP software for performing image analysis and thresholding. Beside the available software, some R libraries have been also created for DHP analysis; examples include the 'caiman' (Diaz and Lencinas 2015) and the 'Hemiphot' (Hans ter Steege 2018) libraries.

[TABLE 4]

(5) Indirect methods such as canopy photography are influenced by woody components (stems and branches) in tree canopies, since passive optical measurements cannot distinguish between leaves and woody elements. Therefore, most indirect methods estimate the plant area index (PAI) rather than actual LAI, because of the contribution of WAI. This issue is more relevant in DHP than in DCP, as WAI increases naturally with zenith angle (Kucharik et al. 1998). A woody-to-total area ratio has been introduced to account for the woody elements' contribution and to separate LAI from PAI (Chen 1996). WAI typically amounts to between 5% and 30% of the total PAI (Yan et al. 2019). The use of near-infrared photography has been tested to separate the contribution of WAI from PAI in passive optical measurements (Zou et al. 2009; Chapman 2007). However, applications using near-infrared photography have been limited, and woody components have rarely been measured in ground experiments because current commercial instruments do not have near-infrared bands (Yan et al. 2019).

(6) Foliage elements are seldom randomly distributed in the canopy, and thus the calculation of clumping index, Ω, is required to correct LAI_e to get the true LAI. In DHP, all the available clumping correction formulae shown in Table 1 can be calculated; however, each clumping correction has its strengths and weaknesses. A recent review (Yan et al. 2019) indicated that in DHP the CC method provides the lowest correction, the LX method provides larger correction than CC, and CLX provides the largest correction, which is generally closer to "true" clumping. The lower performance of CC is due to its inability to detect many small gaps in DHP (Ryu et al. 2010); conversely, this method is particularly suited to DCP, which has a better ability to identify small gaps (Macfarlane et al. 2007a). The LX method is sensitive

to the choice of segment size (Chianucci et al. 2015a) and to segments without gaps, which are particularly critical in denser canopies (Chianucci et al. 2019). The combined CLX method has both of these limitations (Yan et al. 2019). Whatever the method used, the different algorithms and image setups (number and size of segments, zenith angle range) yield different estimates of Ω, thus limiting the comparability among different clumping protocols. Chianucci et al. (2019) recently developed a clumping correction method (LXG) to address the limitations of the established clumping methods in DHP and tested it in medium-dense forest canopies. Results indicated that LXG is relatively insensitive to segment size and provides an estimate of Ω closer to the true value when compared with LX, CC and CLX. Therefore, LXG can represent a valuable option for standardizing the protocol for clumping correction in indirect optical methods.

(7) A main difference between DHP and RVP is that DHP uses fewer pixels in sampling each canopy (either azimuth or zenith) sector, as the largest footprint of the canopy is sampled in a single image. The difference is largest at the zenith, because the number of pixels in DHP decreases at the inner rings, which lessens confidence in the accuracy of CCO estimates from DHP (Chianucci 2016). The number of pixels used in DHP images can be increased by using full-frame hemispherical images (Figure 6) instead of circular hemispherical images (Macfarlane et al. 2007b). Unlike circular images, in which the entire canopy hemisphere is contained in a circle inside the rectangular frame of the image, full-frame hemispherical images have a reduced FOV, such that the full zenith angle range extends to the corners of the rectangular image, increasing the image resolution. The limitation is that the sampling is not uniform across the zenith range (some canopy portions at larger zenith angles are not included in the image). In addition, image analysis software is generally tailored only for circular hemispherical image analysis; the only exception is Winscanopy, which can process both types of hemispherical image (as well as cover images).

[FIGURE 6]

4. Comparison of overstory canopy photographic techniques

4.1 Case study

A case study was performed to illustrate the differences among the overstory canopy photographic techniques, and to propose sampling strategies for overstory canopy structure retrieval.

The trial was conducted in seven 0.25 ha (50 m x 50 m) single-layered beech (*Fagus sylvatica* L.) stands, which were sampled in summer 2018 in central Italy (Alpe di Catenaia, 43°66' N, 11°92'E). Estimates from photography were compared against benchmark values obtained from high-resolution terrestrial laser scanning (TLS) measurements collected in an independent study (Grotti et al. 2020).

In the sampled stands, different silvicultural treatments had been applied, including natural evolution pattern (unthinned control), periodic thinning, and anticipated seed cutting (for details, see Cutini et al. 2015). As a result, the stands varied in stand density (between 108 and 701 trees per hectare) and canopy density (ranging from sparse to medium dense, with effective PAI estimated from TLS ranging between 1.3 and 5.3). Species composition was nearly pure (beech contribution >90% of basal area). Average tree height was about 20 m.

Reference TLS measurements were performed using a phase-shift FARO Focus 3D X130 laser scanner (Faro Technologies Inc., Florida, USA). Table 5 illustrates the scan acquisition setup. Gap fraction was obtained from automated Otsu's (1979) multiple classification of intensity TLS images derived from raw scan data (Figure 7), using a procedure comparable to the standard image analysis processing of digital canopy images (for details, see Grotti et al. 2020).

[TABLE 5]

4.1.1 Camera acquisition and processing of canopy images

Digital photographic measurements in each plot were acquired under overcast sky conditions along a grid of sampling points (Figure 7) using a digital single-lens reflex camera (Nikon D90). The images were acquired in raw format (Nikon NEF). The camera was set in aperture-priority mode, with the aperture set to F10.0; exposure was set to underexpose the image by one stop (REV -1) to improve contrast between sky and canopy pixels (Macfarlane et al. 2014). DHP images were acquired at nine sampling points with the camera equipped with a Sigma 4.5 mm F2.8 fisheye lens (Sigma Corporation of America, Ronkonkoma, NY, US). DCP images were acquired with the camera equipped with an AF Nikkor 50mm 1:1.8 D fixed lens, which yields a FOV of about 30°. Given the lower FOV, the number of DCP images collected for estimation of PAI was greater than the number of DHP images, i.e., 45 DCP

images per plot, of which 9 were collected in the same points as for DHP. Benchmark TLS measurements were collected at the same 9 points used for DHP (Figure 7).

After collection, raw DCP and DHP images were first pre-processed using the 'RAW2JPG' toolbox (Macfarlane et al. 2014). The NEF format was converted to 12-bit linear (demosaiced), uncompressed portable gray map (pgm) format using the 'dcraw' (Coffin 2011) functionality. The blue channel of the pgm image was selected and a linear contrast stretch was applied using the 'imadjust' functionality of the Image Processing Toolbox of Matlab (MathWorks Inc., USA); for DHP, the contrast stretch was based on the pixels within the circular mask only. Images were then converted to 8 bits per channel and saved as JPG files for subsequent analysis. A gamma adjustment was also applied to the raw images (Macfarlane et al. 2014). This pre-processing made it possible to capture the full dynamic range of the image, while enhancing the contrast between gap and canopy pixels (Figure 8).

[FIGURE 8]

Both DCP and DHP images were then classified using the two-corner method of Macfarlane (2011). This method first identifies the unambiguous sky and canopy peaks of the image histogram and then detects the point of maximum curvature to the right of the canopy peak and to the left of the sky peak. Mixed pixels containing a portion of canopy and sky, located between the peaks, were classified with a dual threshold (Macfarlane, 2011; Macfarlane et al. 2014); this procedure yielded a binary image of sky or canopy pixels. The two-corner classification method was implemented using the 'DCP 3.15' toolbox (Macfarlane et al. 2014). In DHP images, the classification was based on the pixels within the circular mask only.

After classification, gap fraction was calculated from the DHP images by dividing the hemisphere of each image into five zenith angle rings, each 15° in size, resulting in a zenith angle range of 0°-75°. Gap fraction for 57° photography was derived from each DHP image using a single zenith angle interval ranging between 52° and 62°. Gap fraction from the DCP images was calculated across the entire image area.

Gap fraction was obtained from classified intensity TLS images by either dividing the images into the same number of zenith bins, with the same zenith bin size and the same zenith angle range as used for fisheye images (for comparison with DHP), either using a single zenith angle interval ranging between 52° and 62° (for comparison with 57° photography).

Gap fraction from photography and TLS was then inverted to get an estimate of effective PAI (PAI_e), defined as the PAI calculated without considering clumping correction, which was

calculated using the Miller theorem (Equation 10a) for both DHP and TLS, while an extinction coefficient of k=0.91 was used for 57° photography. For DCP, the inversion of gap fraction required independent measurement of the extinction coefficient; for this reason, 75 leaf inclination angle measurements were collected from beech trees in proximity to the stands, at a measurement height up to 15 m, using the LP method. Measured θ_L yielded an extinction coefficient of 0.85, which indicates a planophile leaf inclination angle distribution. No attempts were made to correct effective PAI for clumping, as the different formulae employed to calculate Ω might have hindered the comparability of estimates from the different instruments and methods. Similarly, no woody corrections were performed to convert PAI to LAI, as the different FOV of the methods would have implied different calculation of WAI (Kucharik et al. 1998). Table 6 summarize the main parameters used for the three canopy photographic techniques.

4.1.2 Comparison of overstory canopy photography techniques

Because of the different FOV of the overstory canopy photographic techniques, the first step was comparison of gap fraction at the first zenith ring (P_0; 0-15° zenith angle range) from DHP and from DCP. Estimates of P_0 from the two photographic methods were significantly correlated ($P_{0\,(DHP)}$=0.72 $P_{0\,(DCP)}$+0.05, R^2= 0.65, $p < 0.001$), but DHP estimated significantly lower P_0 than DCP (ANOVA, $p < 0.001$; Figure 9). Comparison with P_0 estimates derived from TLS at the same 0-15° zenith angle range further confirmed that DCP outperformed DHP at the FOV considered, based on the higher coefficient of determination, the slope closer to unity, and the intercept closer to zero of the regression:

$$P_{0(DHP)} = 0.74\ P_{0(TLS)} + 0.10,\ R^2 = 0.62,\ p < 0.001$$

$$P_{0(DCP)} = 0.97\ P_{0(TLS)} + 0.07,\ R^2 = 0.87,\ p < 0.001$$

[FIGURE 9]

Gap fraction estimated close to 57° (52°-62°) from 57° photography (P_1) was correlated with that obtained from TLS at the same view ($P_{1(57°)} = 1.12\ P_{1(TLS)} + 0.09$, $R^2 = 0.49$, $p < 0.001$), but 57° photography systematically overestimated P_1 compared with TLS (ANOVA, $p <$ 0.001).

Estimated gap fraction obtained from the photographic techniques (at their different zenith angle ranges) were then inverted to get an estimate of PAI_e, which was compared with that measured from TLS at the 0-75° zenith angle range. Regression results indicated that all the photographic methods provided PAI_e estimates correlated with the benchmark values obtained from TLS:

$$PAI_{e(DHP)} = 0.60\ PAI_{e(TLS)} + 0.28,\ R^2 = 0.73,\ p < 0.001$$

$$PAI_{e(DCP)} = 0.71\ PAI_{e\ (TLS)} - 0.07,\ R^2 = 0.72,\ p < 0.001$$

$$PAI_{e(57°)} = 0.48\ PAI_{e\ (TLS)} + 0.32,\ R^2 = 0.74,\ p < 0.001$$

Overall, DCP outperformed the other methods, as its PAI_e regression with TLS had a slope closer to unity and an intercept closer to zero than those of the other photographic methods. Closer inspection revealed that DCP estimated larger values in denser canopies (PAI_e >2) and smaller values in sparser canopies (PAIv < 2) relative to DHP (Figure 9). The poorest results were obtained using 57° photography (Figure 10).

[FIGURE 10]

4.1.3 Outlining strategies for sampling overstory canopy

The comparison indicated that DCP is particularly suited for retrieving gap fraction in medium-dense forest canopies, which are tipically dominated by small gaps (Chen and Cihlar 1995; Song et al. 2018), as DCP's higher ability to detect within-crown gaps allows more accurate canopy gap retrieval close to the zenith. By contrast, DHP has fewer pixels at smaller zenith angles, which results in a lower ability to detect small gaps close to the zenith, resulting in a canopy cover measurement that is intermediate between those of the crown and foliage cover (Chianucci 2016; Pekin and Macfarlane 2009). Therefore, DHP is less suited to denser canopies, which are characterized by smaller gap fraction, as hemisphere portions with no gaps gave undefined results when gap fraction was inverted to estimate PAI. With reference to PAI_e, the lower performance of DHP relative to DCP can also be attributed to the lower ability of DHP to detect smaller canopy elements with increasing optical distance, which results in an underestimation of PAI_e in comparison with TLS, as observed in the previous study (Grotti et al. 2020). The disadvantage of DCP relative to DHP is that estimates of LAI/PAI from DCP

require independent measurements of leaf inclination angle to parametrize *k*. In the case study described, reliable PAI_e estimates were obtained from DCP using measured leaf inclination angles collected in sample trees, which indicates a planophile leaf inclination distribution. However, closer inspection of the results suggested that sparser canopies have more inclined leaves, while denser canopies have more horizontal (planophile) distribution; this result is in accordance with a previous study, which observed that mean leaf inclination in beech decreases with increasing canopy density (Liu et al. 2019). In addition, beech trees generally have more inclined leaves at the top of the canopy and more horizontal leaves at the bottom of the canopy (Liu et al. 2019); this may have resulted in a more horizontal estimation of leaf inclination distribution, since levelled measurements have been mainly concentrated at more accessible lower canopy height. Results confirmed the importance of measuring leaf inclination in the field to improve estimation of LAI/PAI from DCP.

The 57° method showed larger underestimation of PAI_e than the other photographic methods. This method has the advantage that *k* is certain (Figure 1) and that the measurements can be derived from the DHP images. Owing to the greater path length, the overall gap fraction is smaller at 57° than at the zenith, and therefore more images are needed to prevent undersampling in denser canopies, which are characterized by smaller gap fraction. In the case study, 57° images were not conceived in the original sampling design and were thus derived from DHP images; the limited number of 57° images used for the analysis may have exaggerated the undersampling in the canopies considered. The use of more images is therefore generally recommended when the 57° method is used in denser canopies. In addition, woody materials increase with increasing zenith angle; thus in the case study the LAI_e obtained from 57° photography may be more underestimated than that obtained with the other methods, as woody corrections were not performed.

Owing to the differences between the DCP and DHP, there is no *a priori* reason to consider one method superior to the other; rather, their different features may support their use in different conditions. The restricted FOV and the rectangular shape of cover images makes DCP particularly suited for calibrating and validating optical remotely sensed information, which generally has comparable FOV with DCP. In addition, the greater accuracy with which DCP measures canopy cover makes this method particularly suited for measuring canopy cover attributes (FCO and CCO), without requiring knowledge about θ_L and $f(\theta_L)$. Finally, DCP is less sensitive to light condition and camera exposure, and therefore it can be used routinely in

common working hours. By contrast, DHP can be used to estimate PAI or LAI in situations where measurements of θ_L are lacking or difficult to perform. Both methods could be used together to maximize their different advantages: For instance, DHP could be used to obtain an estimate of LAI and k in reference plots. DCP could then be applied more routinely to large numbers of plots based on the calculated k value.

With reference to image acquisition and processing, the comparison indicated that shooting in raw mode and applying a linear contrast stretch is an effective procedure for standardizing and optimizing the camera acquisition protocol, while minimizing the influence of camera exposure (Macfarlane et al. 2014). Based on the results of the case study, the general recommendations for image acquisition and processing are as follows:

i. Acquire images in diffuse sky conditions.
ii. Set the exposure to underexpose by on one or two stops (relative exposure value: -1 or -2) with the camera in aperture-priority mode and with small aperture (large F-value).
iii. Shoot in raw mode (when available from the camera).
iv. Check the shooting results in the field using the camera histogram. The best exposure should have high dynamic range and no saturation at either end of the histogram.
v. Apply a linear contrast stretch, possibly prior to conversion from raw to viewable image format (if raw mode is available from the camera).
vi. Select the appropriate camera channel and image classification method. The blue channel is generally used for classification. Automated classification is recommended over manual classification.
vii. When using DHP, perform lens correction (often available from image analysis software). Select an appropriate number of zenith rings and azimuth sectors for calculating gap fraction. The ring and azimuth size should be small enough to meet the random distribution assumption, but large enough to avoid empty segments (Chianucci et al. 2015a). Outer hemispherical portions are generally noisy, and therefore the zenith angle range is often restricted (e.g. 0°-75°).
viii. When using DCP, select a method for classifying gap fraction into large and small gaps; automated classification is recommended over manual classification. Select or measure the appropriate k when the target is to estimate LAI. Lens correction is also

recommended.

ix. Select an appropriate LAI algorithm to invert gap fraction.

With reference to the sampling effort, the proposed number of optical measurements is determined by the different FOV of the photographic lenses employed in the different methods. The number of measurements adopted in the case study (9 for DHP and 45 for DCP) was suitable considering the plot size and the relatively dense canopy sampled, in accordance with previous reports (Calders et al. 2018; Chianucci et al. 2015a), while more measurements would have been advisable for 57° photography; for example, Macfarlane et al. (2007c) suggested collecting thirty-two 57° images for a stand area of 0.25 ha. More measurements are generally recommended in sparser canopies, which are dominated by between-crown gaps. For instance, in a systematic comparison of different sampling designs when using LAI-2000 in boreal forests characterized by sparse to medium-dense canopies, Majasalmi et al. (2012) concluded that 12 randomly located measurement points were suitable for characterizing LAI for a stand area of 0.13 ha; the accuracy improved when the 12 sampling points were systematically distributed. A similar design can be recommended for sampling of sparser canopies using DHP.

5. Other canopy photography applications

The following paragraphs illustrate emerging fields of *in situ* canopy photography beyond the established overstory canopy applications.

5.1 *Understory photography*

Some studies have shown that the understory LAI may exceed that of the overstory (Law et al. 2001; Macfarlane et al. 2010). Failure to account for the understory can reduce the accuracy of remotely sensed estimates of LAI (Eriksson et al. 2006). However, very few attempts have been made to estimate the LAI of the forest understory.

Macfarlane and Ogden (2012) pioneered an understory photographic method in which the CCO of understory vegetation is estimated from nadir images acquired using a camera equipped with a short lens mounted on an extendable pole (2-10 m) and oriented downward. This method can be considered an "upside-down" version of DCP. The major challenge compared to upward-facing photographic methods is that image analysis is more complex, as it requires colour image analysis of the forest floor. The forest understory may contain many

different plant species, combined with the presence of a spectrally complex background against which to extrapolate plant canopies (Macfarlane and Ogden 2012). In addition, dead leaves and litter can obscure underlying vegetation; thus it may be necessary to remove background elements prior to collecting measurements. The digital image format has some desired features for analysing understory vegetation. Indeed, the R,G,B bands can be used to classify vegetation using visible vegetation indices; this option has been frequently tested in crops and weeds (Chianucci et al. 2018a; Liu et al. 2013; Meyer and Neto 2008).

Macfarlane and Ogden (2012) processed nadir images using a combination of a green vegetation index (GLA) and a colour space conversion (CIELAB; Figure 11). Among seven methods tested, the authors suggested the use of the "LAB2" method for dense canopies (cover > 0.1) and the "Rosin" method for sparse canopies (cover < 0.1). Song et al. (2015) proposed an improvement of the LAB2 method to adjust the classification of shaded pixels. Salas-Aguilar et al. (2017) proposed an alternative classification method specifically tailored for understory vegetation, based on CIELAB colour space conversion and threshold optimization.

[FIGURE 11]

5.2 Photography for phenological monitoring

While satellite optical remote sensing has frequently been used for monitoring vegetation phenology, the temporal and spatial resolution is often not suitable for detecting stand-scale phenological events (Sonnentag et al. 2012). In addition, multitemporal satellite monitoring requires accurate calibration with repeated field data. For this reason, digital photography has been widely used to monitor the phenology of forest canopies at the tree and stand scales (Sonnentag et al. 2012). Camera phenological monitoring systems are generally based on automatic acquisition camera, which are generally oriented downward or inclined; phenological transitions in vegetation are assessed by measuring variation in vegetation indices derived from repeated photographs. Upward-looking cameras (DCP, DHP) have also been tested (e.g., Ryu et al. 2012; Lang et al. 2017), but they are less frequently used in phenological monitoring than downward or inclined photography.

The cameras adopted in phenological monitoring can feature a near-infrared (NIR) channel (Nakaji et al. 2011), but consumer grade RGB cameras are more often used (Nagai et al. 2016). The RGB data are converted to greenness indices to quantify the seasonal vegetation

changes; the most widely used indices are the green excess index (GEI=2G-R-B; Richardson et al. 2007; Saitoh et al. 2012; Nagai et al. 2014) and the green chromatic coordinate index (Gcc=G/(R+G+B); Sonnentag et al. 2012).

Examples of camera phenological monitoring networks are PhenoCam (Richardson et al. 2007), which collects images across the United States and adjacent Canada, and the Phenological Eyes Network (PEN), which collected images in Asia, mainly in Japan (Nasahara and Nagai 2015).

5.3 Individual-tree and urban tree photographic approaches

Early photographic attempts to estimate individual tree leaf area were carried out in the 1980s and can be grouped into two categories. The first is based on perspective photographic images, which can be classified as a close-range photogrammetric approach. Examples of this approach have been given in Van Elsacker et al. (1983), Peper and McPherson (2003) and Phattaralerphong et al. (2006). The other group comprises hemispherical view photographic approaches, as first proposed by Koike (1985), to derive leaf area density of individual trees. More recently, upward-oriented RVP methods have been tested for individual tree measurements (Chianucci et al. 2015b).

Optical measurement of urban trees poses further challenges, as the proximity of trees to infrastructure elements can strongly affect the accuracy of tree canopy analysis. In such cases, urban tree leaves can be separated from nearby buildings (see example in Figure 12) using vegetation indices, either involving near-infrared (Osmond 2009) or visible bands (Chianucci et al. 2015b; Van Monteiro et al. 2018).

[FIGURE 12]

5.4 Smartphone photography and applications

RVP has favoured the extension of canopy photography to smartphones (and also mobile tablets). While the current high quality of smartphone cameras makes it possible to use them as an alternative to standard point-and-shoot cameras (Bianchi et al. 2017; Chianucci et al. 2018a; Smith and Ramsay 2018), smartphone technology has several further advantages. In terms of hardware capabilities, the smartphone camera can be integrated with many different sensors, which makes it possible to measure the orientation and position of the acquired images

from inertial and GPS sensors, and allows data transmission through wifi/bluetooth communication protocols. In terms of software capabilities, the smartphone technology allows the development of specific software packages that can be designed to run on these devices ("apps"). A specific app can be designed to use the available smartphone (camera and other) sensors to fulfil specific objectives.

An example of a canopy application is the PocketLAI (Confalonieri et al. 2013); using this app, the camera accelerometer can capture images when the camera sensor reaches 57.5°, and then a segmentation is applied to produce a binary classification, which is used to estimate LAI from classified gap fraction. Other apps have been specifically developed for retrieving canopy structure from either downward-looking (Canopeo, CCO Free) or upward-looking images (Habit app, Canopy app, LAICanopy). By connecting two smartphone terminals, Qu et al. (2016) designed an integrated measurement system, LAISmart, which provides two image segmentation options based on either the greenness index or the blue band intensity of respectively downward- and upward-looking smartphone images. LAI is then estimated from the gap fraction model assuming a spherical leaf angle distribution. The integrated system uses wifi to transfer data to a remote computer server, thus reducing the cost of field data collection.

From a wider point of view, smartphone technology allows instant information gathering and sharing, which can lead towards the use of smartphones as a tool for collecting photographic data and implementing them in a citizen science framework. An example of this approach is the use of smartphone photography to monitor phenology (Hufkens et al. 2019). Digital Earth Watch (DEW) and the Picture Post Network are an example of a citizen science project for phenological monitoring which is based on digital camera or smartphone photographs acquired by visitors at local markers in fixed orientations; the network makes it possible to obtain a standardized series of digital images for observing and measuring changing vegetation over time (Graham et al. 2011). The possibility to collect the position of acquired smartphone images also holds great potential for ground truthing and calibrating remotely sensed information through collections of georeferenced images.

6. Discussion and conclusions

Since the discovery of the ingenious fisheye lens, the technology, techniques and applications of photography for forest canopy studies have developed greatly. The digital image format has strongly facilitated image acquisition procedures and image processing. The

development of dedicated software, combined with the lower price of the cameras in comparison with other optical sensors, have resulted in widespread adoption of canopy photography in the scientific community. Recent advances in image analysis methods have further reduced the drawbacks of image acquisition and processing. The use of digital cameras with restricted view (and often fixed) lenses, as in RVP, has entailed a second phase of development in canopy photography, favouring the introduction of new approaches and extending the applicability of photography to new sensors and platforms, including smartphones. These developments have made it possible to address many previous challenges, including within-crown clumping correction (Macfarlane et al. 2007b,c), measurement of isolated and urban trees (Chianucci et al. 2015b), operational leaf inclination angle measurement (Ryu et al. 2010; Pisek et al. 2013), phenological assessment (Lang et al. 2017; Smith and Ramsay 2018), post-disturbance monitoring of canopy recovery (Toda et al. 2018), and estimation of understory LAI (Chianucci et al. 2014b).

These improvements notwithstanding, canopy photography still has some major issues associated with the lack of standardization in field protocols, the dependence of the results on sky conditions and camera exposure. While recent and future advances in raw photography may strongly reduce the issue of camera exposure (Macfarlane et al. 2014; Hwang et al. 2016; Grotti et al. 2020), the current main challenges in using canopy photography are the following:

1) With reference to field protocols for LAI, efforts to standardize the procedure for image acquisition and processing have mostly focused on DHP. More studies are needed to make other canopy photographic techniques such as DCP operational in ground-based canopy measurement protocols.

2) Relatively few attempts have been made to derive $f(\theta_L)$ in the field, owing to the lack of convenient operational methods (Yan et al. 2019). LP can significantly help to bridge this gap. The use of UAV can further improve use of LP for acquiring images at treetop height and makes it possible to measure θ_L along the vertical tree-height profile (McNeill et al. 2016). Further efforts are required to increase the automation of the photographic measurement of θ_L (currently, θ_L are measured manually from LP). As LP is suited for broadleaved species, operational solutions are still required for coniferous species.

3) Although canopy photography has been used to measure WAI in trials, more efforts are still needed to improve its convenience in field measurements (Yan et al. 2019). Thermal or multispectral photography could potentially make *in situ* WAI measurements operational (Kirby et al. 2018; Noelke et al. 2015; Zou et al. 2009), but such options needs further testing.

While active field technologies such as (aerial and terrestrial) laser scanning are opening new frontiers in measurement of the three-dimensional structure of forests, digital photography still represents the cheapest, simplest and quickest solution and is currently the most suitable tool for routine measurements and monitoring of canopy attributes in forest stands.

Advances in information and communications technology (ICT) hold great potential to further extend the use of canopy photography because of i) the cheap and widespread ownership of standard and smartphone cameras; ii) the increasing availability of free software, free language programming and libraries and apps to process images, which also make canopy photography accessible to non-experts; iii) developments in smartphone technology offering a powerful combination of sensors, information transfer and computing power which is expected to advance exploitation of smartphone technology in research; and iv) the increasing use of technology in citizen science frameworks, which potentially allow the collection of information at high temporal frequency and wider spatial coverage, demonstrating the potential for real-time information flows among collectors, databases, interpreters and users of information (Fardusi et al. 2017; Teacher et al. 2013).

Acknowledgements I am indebted with Dr. Craig Macfarlane for kindly share its routines for image analysis and processing. I am grateful to the anonymous referees and editor, which helped to improve the manuscript with their comments. The study has been financially supported by the research project PRECISIONPOP (Sistema di monitoraggio multiscalare a supporto della pioppicoltura di precisione nella Regione Lombardia) funded by the Lombardy Region.

References

Alivernini, A., Fares, S., Ferrara, C., Chianucci, F. 2018. An objective image analysis method for estimation of canopy attributes from digital cover photography. Trees 32(3): 713-723.

Anderson, M.C. 1964. Studies of the woodland light climate I. The photographic computation of light condition. Journal of Ecology 52: 27-41.

Anderson, M.C. 1971. Radiation and crop structure. In: Sestak, Z., Catsky, J., Jarvis, P.G., (eds.) Plant photosynthetic Production Manual of Methods. Junk, the Hague: 77-90.

Anderson, M.C. 1981. The geometry of leaf distribution in some south-eastern Australian forests. Agricultural Forest Meteorology 25:195-205.

872 Andis, A.Z. 2018. Taking hemispherical canopy photos [online]. Avaliable from:
873 https://www.azandisresearch.com/2018/07/24/taking-hemispherical-canopy-photos
874 [Accessed 17 March 2019].
875 Angelini, A., Corona, P., Chianucci, F. and Portoghesi, L., 2015. Structural attributes of stand
876 overstory and light under the canopy. Annals of Silvicultural Research 39: 23-31. Doi:
877 10.12899/ASR-993
878 Baret, F., Weiss, M ., Allard, D., Garrigues, S., Leroy, M., et al. 2008. VALERI: a network of
879 sites and a methodology for the validation of medium spatial resolution land satellite
880 products. Remote Sensing of Environment 76(3): 36-39.
881 Beckschäfer, P., Seidel, D., Kleinn, C., Xu, J. 2013. On the exposure of hemispherical
882 photographs in forests. iForest-Biogeosciences and Forestry 6(4): 228-237.
883 Bianchi, S., Cahalan, C., Hale, S., Gibbons, J.M. 2017. Rapid assessment of forest canopy and
884 light regime using smartphone hemispherical photography. Ecology and evolution, 7(24):
885 10556-10566.
886 Bonhomme, R., Chartier, P. 1972. The interpretation and automatica measurement of
887 hemispherical photographs to obtain sunlit foliage area and gap frequency. Israel J. Agric.
888 Res. 22: 53-61.
889 Bréda, N. 2003. Ground-based measurements of leaf area index: a review of methods
890 instruments and current controversies. J. Exp. Bot. 54: 2403–2417.
891 Calders, K., Origo, N., Disney, M., Nightingale, J., Woodgate, W., Armston, J. and Lewis, P.,
892 2018. Variability and bias in active and passive ground-based measurements of effective
893 plant, wood and leaf area index. Agricultural and forest meteorology, 252: 231-240.
894 Campbell, G.S., Norman, J.M., 1989. The description and measurement of plant canopy
895 structure. In: Russell, G., Marshall, B., Jarvis, P.G. (Eds.), Plant Canopies: Their Growth,
896 Form and Function. Cambridge University Press, Cambridge, UK, pp. 1–19.
897 Cescatti, A. 2007. Indirect estimates of canopy gap fraction based on the linear conversion of
898 hemispherical photographs. Methodology and comparison with standard thresholding
899 techniques. Agricultural and Forest Meteorology 143: 1-12.
900 Chan, S.S., McCreight, R.W., Walstad, J.D., Spies, T.A. 1986. Evaluating forest vegetative
901 cover with computerized analysis of fisheye photographs. Forest Science 32: 1085-1091.
902 Chapman, L. 2007. Potential applications of near infra-red hemispherical imagery in forest
903 environments. Agricultural and Forest Meteorology, 143(1-2): 151-156.

904 Chen, J.M. 1996. Optically-based methods for measuring seasonal variation of leaf area index
905 in boreal conifer stands. Agricultural and Forest Meteorology 80 (2-4): 135-163.
906 Chen, J.M., Black, T.A. 1992. Defining leaf area index for non-flat leaves. Plant Cell
907 Environ. 15: 421-529.
908 Chen, J.M., Black, T.A., Adams, R.S. 1991. Evaluation of hemispherical photography for
909 determining plant area index and geometry of a stand. Agricultural and Forest Meteorology
910 56: 129-132.
911 Chen, J.M., Cihlar, J. 1995. Quantifying the effect of canopy architecture on optical
912 measurements of leaf area index using two gap size analysis methods. IEEE T. Geosci.
913 Remote Sens. 33: 777-787.
914 Chen, J.M., Rich, P.M., Gower, S.T., Norman, J.M., Plummer, S. 1997. Leaf area index of
915 boreal forests: theory, techniques, and measurements. Journal of Geophysical Research 102
916 (D24): 29429-29443.
917 Chianucci, F., 2016. A note on estimating canopy cover from digital cover and hemispherical
918 photography. Silva Fennica, 50(1): 1-10.
919 Chianucci, F., Cutini, A. 2012. Digital hemispherical photography for estimating forest canopy
920 properties: current controversies and opportunities. iForest 5: 290-295.
921 Chianucci, F., Cutini, A., 2013. Estimation of canopy properties in deciduous forests with
922 digital hemispherical and cover photography. Agricultural and Forest Meteorology 168:
923 130-139.
924 Chianucci, F., Cutini, A., Corona, P., Puletti, N. 2014a. Estimation of leaf area index in
925 understory deciduous trees using digital photography. Agricultural and Forest Meteorology
926 198: 259-264.
927 Chianucci, F., Disperati, L., Guzzi, D., Bianchini, D., Nardino, V., Lastri, C., Rindinella, A.
928 and Corona, P., 2016. Estimation of canopy attributes in beech forests using true colour
929 digital images from a small fixed-wing UAV. International Journal of Applied Earth
930 Observation and Geoinformation, 47, pp.60-68.
931 Chianucci, F., Macfarlane, C., Pisek, J., Cutini, A., Casa, R. 2015a. Estimation of foliage
932 clumping from the LAI-2000 Plant Canopy Analyzer: effect of view caps. Trees 29(2): 355-
933 366.
934 Chianucci F, Pisek J, Raabe K, Marchino L, Ferrara C, Corona P (2017). A dataset of leaf
935 inclination angles for temperate and boreal broad- leaf woody species. Mendeley Data, V2,
936 [Dataset], https://doi.org/ 10.17632/4rmc7r8zvy.2

Chianucci, F., Pisek, J., Raabe, K., Marchino, L., Ferrara, C., Corona, P. 2018b. A dataset of leaf inclination angles for temperate and boreal broadleaf woody species. Annals of Forest Science 75(2), p.50.

Chianucci, F., Puletti, N., Giacomello, E., Cutini, A., Corona, P. 2015b. Estimation of leaf area index in isolated trees with digital photography and its application to urban forestry. Urban Forestry & Urban Greening 14(2): 377-382.

Chianucci, F., Puletti, N., Venturi, E., Cutini, A., Chiavetta, U. 2014b. Photographic assessment of overstory and understory leaf area index in beech forests under different management regimes in Central Italy. Forestry Studies 61(1): 27-34.

Chianucci, F., Zou, J., Leng, P., Zhuang ,Y., Ferrara, C. 2019. A new method to estimate clumping index integrating gap fraction averaging with the analysis of gap size distribution. Canadian Journal of Forest Research, *(early view)*, doi: 10.1139/cjfr-2018-0213

Chianucci, F., Lucibelli, A., Dell'Abate, M.T. 2018a. Estimation of ground canopy cover in agricultural crops using downward looking photography. Biosystems Engineering 169: 209-216.

Coffin, D. (2011). DCRAW: Decoding raw digital photos in linux.

Confalonieri, R., Foi, M., Casa, R., Aquaro, S., Tona, E., Peterle, M., Boldini, A., De Carli, G., Ferrari, A., Finotto, G. and Guarneri, T., 2013. Development of an app for estimating leaf area index using a smartphone. Trueness and precision determination and comparison with other indirect methods. Computers and Electronics in Agriculture 96: 67-74.

Costa, C., Figorilli, S., Proto, A.R., Colle, G., Sperandio, G., Gallo, P., Antonucci, F., Pallottino, F., Menesatti, P. 2018. Digital stereovision system for dendrometry, georeferencing and data management. Biosystems Engineering, 174: 126-133.

Dawson, T.P., Curran, P.J., North, P.R.J., Plummer, S.E. 1999. The propagation of foliar biochemical absorption features in forest canopy reflectance: A theoretical analysis. Remote Sensing of Environment 67(2): 147-159.

de Wit, C.T. 1965. Photosynthesis of Leaf Canopies. Agricultural Reports No. 663. PUDOC, Wageningen, the Nederlands.

Diaz, G.M., Lencinas, J.D., 2015. Enhanced Gap Fraction Extraction From Hemispherical Photography. IEEE Geosci. Remote Sens. Lett. 12, 1784-1789….

Eriksson, H.M., Eklundh, L., Kuusk, A. and Nilson, T., 2006. Impact of understory vegetation on forest canopy reflectance and remotely sensed LAI estimates. Remote Sensing of Environment 103(4): 408-418.

970 Evans, G.C., Coombe, D.E. 1959. Hemisperical and woodland canopy photography and the
971 light climate. Journal of Ecology, 47(1): 103-113.
972 Fardusi, M.J., Chianucci, F. and Barbati, A., 2017. Concept to practice of geospatial-
973 information tools to assist forest management and planning under precision forestry
974 framework: a review. Annals of Silvicultural Research, 41(1): 3-14.
975 Fleck, S., Raspe, S., Cater, M., Schleppi, P., Ukonmaanaho, L., Greve, M., Hertel, C., Weis,
976 W., Rumpf, S., Thimonier, A., Chianucci, F., Beckschäfer, P., 2016: Part XVII: Leaf Area
977 Measurements. In: UNECE ICP Forests Programme Co-ordinating Centre (ed.): Manual on
978 methods and criteria for harmonized sampling, assessment, monitoring and analysis of the
979 effects of air pollution on forests. Thünen Institute of Forest Ecosystems, Eberswalde,
980 Germany, 34 pp. https://www.icp-
981 forests.org/pdf/manual/2016/ICP_Manual_2016_01_part17.pdf
982 Fuentes, S., De Bei, R., Pozo, C. and Tyerman, S., 2012. Development of a smartphone
983 application to characterise temporal and spatial canopy architecture and leaf area index for
984 grapevines. Wine Vitic. J. 6: 56-60.
985 Glatthorn, J., Beckschäfer, P. 2014. Standardizing the protocol for hemispherical photographs:
986 accuracy assessment of binarization algorithms. PloS one, 9(11), p.e111924.
987 Goel, N.S., Strebel, D. 1984. Simple beta distribution representation of leaf orientation in
988 vegetation canopies. Agron. J. 76: 800 - 802.
989 Gonsamo, A., D'Odorico, P. and Pellikka, P. 2013. Measuring fractional forest canopy element
990 cover and openness–definitions and methodologies revisited. Oikos, 122(9): 1283-1291.
991 Goudriaan, J. 1988. The bare bones of leaf-angle distribution in radiation models for canopy
992 photosynthesis and energy exchange. Agric. Forest Meteorol. 43, 155-169
993 Graham, E.A., Henderson, S. and Schloss, A., 2011. Using mobile phones to engage citizen
994 scientists in research. Eos, Transactions American Geophysical Union, 92(38), pp.313-315.
995 Grotti, M., Calders, K., Origo, N., Puletti, N., Alivernini, A., Ferrara, C., Chianucci, F. 2020.
996 An intensity, image-based method to estimate gap fraction, canopy openness and effective
997 leaf area index from phase-shift terrestrial laser scanning. Agricultural and Forest
998 Meteorology, 280, 107766.
999 Hill, R. 1924. A lens for Whole Sky Photographs, Quarterly Journal of the Royal
1000 Meteorological Society, Vol. 50: 227-235, 1924

1001 Hufkens, K., Melaas, E.K., Mann, M.L., Foster, T., Ceballos, F., Robles, M. and Kramer, B.,
1002 2019. Monitoring crop phenology using a smartphone based near-surface remote sensing
1003 approach. Agricultural and Forest Meteorology, 265, pp.327-337.
1004 Hwang, Y., Ryu, Y., Kimm, H., Jiang, C., Lang, M., Macfarlane, C., Sonnentag, O. 2016.
1005 Correction for light scattering combined with sub-pixel classification improves estimation
1006 of gap fraction from digital cover photography. Agricultural and Forest Meteorology 222:
1007 32-44.
1008 ICOS, 2014. Protocol Ancillary Data in Forests. In: Gielen, B., Beeck, M.O.d. (Eds.).
1009 Jennings, S.B., Brown, N.D., Sheil, D. 1999. Assessing forest canopies and understorey
1010 illumination: canopy closure, canopy cover and other measures. Forestry: An International
1011 Journal of Forest Research 72(1): 59-74.
1012 Jonckheere, I., Fleck, S., Nackaerts, K, Muys, B., Coppin, P., Weiss, M., Baret, F., 2004.
1013 Review of methods for in situ leaf area index determination: Part I. Theories sensors and
1014 hemispherical photography. Agricultural and Forest Meteorology 121: 19-35.
1015 Jonckheere, I., Nackaerts, K., Muys, B., Coppin, P. 2005. Assessment of automatic gap fraction
1016 estimation of forests from digital hemispherical photography. Agricultural and Forest
1017 Meteorology 132: 96–114.
1018 Kirby, J., Chapman, L. and Chapman, V., 2018. Assessing the Raspberry Pi as a low-cost
1019 alternative for acquisition of near infrared hemispherical digital imagery. Agricultural and
1020 forest meteorology, 259: 232-239.
1021 Kobayashi, H., Ryu, Y., Baldocchi, D.D., Welles, J.M., Norman, J.M. 2013. On the correct
1022 estimation of gap fraction: How to remove scattered radiation in gap fraction
1023 measurements?. Agricultural and Forest Meteorology 174: 170-183.
1024 Koike, F., 1985. Reconstruction of two-dimensional tree and forest canopy profiles using
1025 photographs. Journal of Applied Ecology: 921-929.
1026 Kucharik, C.J., Norman, J.M., Gower, S.T., 1998. Measurements of branch area and adjusting
1027 leaf area index indirect measurements. Agric. For. Meteorol. 91, 69–88.Kuusk, A., Lang,
1028 M. and Kuusk, J., 2013. Database of optical and structural data for the validation of forest
1029 radiative transfer models. In Light Scattering Reviews 7: 109-148, Springer Berlin
1030 Heidelberg.
1031 Landini, G., Randell, D.A., Fouad, S., Galton, A., 2017. Automatic thresholding from the
1032 gradients of region boundaries. Journal of microscopy, 265(2): 185-195.

1033 Lang, A.R.G., Xiang, Y. 1986. Estimation of leaf area index from transmission of direct
1034 sunlight in discontinuous canopies. Agricultural and Forest Meteorology 35: 229–243.
1035 Lang, M., Kuusk, A., Mõttus, M., Rautiainen, M., Nilson, T. 2010. Canopy gap fraction
1036 estimation from digital hemispherical images using sky radiance models and a linear
1037 conversion method. Agricultural and Forest Meteorology, 150(1): 20-29.
1038 Lang, M., Nilson, T., Kuusk, A., Pisek, J., Korhonen, L., Uri, V. 2017. Digital photography for
1039 tracking the phenology of an evergreen conifer stand. Agricultural and Forest Meteorology,
1040 246: 15-21.
1041 Law, B.F., S. Van Tuyl, A. Cescatti and D. D. Baldocchi. 2001. Estimation of leaf area index
1042 in open-canopy ponderosa pine forests at different successional stages and management
1043 regimes in Oregon. Agricultural and Forest Meteorology 108: 1 - 14.
1044 Leblanc, S.G., Chen, J.M., Fernandes, R., Deering, D.W., Conley, A. 2005. Methodology
1045 comparison for canopy structure parameters extraction from digital hemispherical
1046 photography in boreal forests. Agricultural and Forest Meteorology 129: 187-207.
1047 Leblanc, S.G. 2002. Correction to the plant canopy gap-size analysis theory used by the tracing
1048 radiation and architecture of canopies instrument. Applied Optics 41:7667 - 7670.
1049 Liu, J., Pattey, E., Admiral, S. 2013. Assessment of in situ crop LAI measurement using
1050 unidirectional view photography. Agricultural and Forest Meteorology 160: 9, 25 - 34.
1051 Liu, J., Skidmore, A.K., Wang, T., Zhu, X., Premier, J., Heurich, M., Beudert, B. and Jones,
1052 S., 2019. Variation of leaf angle distribution quantified by terrestrial LiDAR in natural
1053 European beech forest. ISPRS journal of photogrammetry and remote sensing, 148,
1054 pp.208-220.
1055 Macfarlane, C. 2011. Classification method of mixed pixels does not affect canopy metrics
1056 from digital images of forest overstorey. Agricultural and Forest Meteorology 151: 833-
1057 840.
1058 Macfarlane, C., Arndt, S.K., Livesley, S.J,, Edgar, A.C., White, D.A., Adams, M.A., Eamus,
1059 D. 2007a. Estimation of leaf area index in eucalypt forest with vertical foliage, using cover
1060 and fullframe fisheye photography. For. Ecol. Manage. 242: 756-763.
1061 Macfarlane, C., Coote, M., White, D.A., Adams, M.A. 2000. Photographic exposure affects
1062 indirect estimation of leaf area in plantations of Eucalyptus globulus Labill. Agricultural
1063 and Forest Meteorology 100:155–168. doi: 10.1016/S0168-1923(99)00139-2

1064 Macfarlane, C., Grigg, A., Evangelista, C. 2007b. Estimating forest leaf area using cover and
1065 fullframe fisheye photography: Thinking inside the circle. Agricultural and Forest
1066 Meteorology 146: 1-12.
1067 Macfarlane, C., Hoffman, M., Eamus, D., Kerp, N., Higginson, S., McMurtrie, R., Adams,
1068 M.A. 2007c. Estimation of leaf area index in eucalypt forest using digital photography.
1069 Agric. For. Meteorol.143: 176–188.
1070 Macfarlane, C., Ogden, G.N. 2012. Automated estimation of foliage cover in forest understorey
1071 from digital nadir images. Methods in Ecology and Evolution 3: 405 - 415.
1072 Macfarlane, C., Ryu, Y., Ogden, G.N., Sonnentag, O. 2014. Digital canopy photography:
1073 Exposed and in the raw. Agricultural and Forest Meteorology 197: 244-253.
1074 Macfarlane, C., Lardner, T., Patterson, K., Grigg, A.H., 2010 A new model for predicting
1075 understorey leaf area from biomass in eucalypt forest to test the ecohydrological equilibrium
1076 theory. Methods in Ecology and Evolution, 1: 371 - 379.
1077 Majasalmi, T., Rautiainen, M., Stenberg, P. and Rita, H., 2012. Optimizing the sampling
1078 scheme for LAI-2000 measurements in a boreal forest. Agricultural and Forest
1079 Meteorology, 154: 38-43.
1080 Marra, E., Cambi, M., Fernandez-Lacruz, R., Giannetti, F., Marchi, E., Nordfjell, T. 2018.
1081 Photogrammetric estimation of wheel rut dimensions and soil compaction after increasing
1082 numbers of forwarder passes. Scandinavian Journal of Forest Research, 33(6): 613-620.
1083 McNeil, B.E., Pisek, J., Lepisk, H. and Flamenco, E.A., 2016. Measuring leaf angle distribution
1084 in broadleaf canopies using UAVs. Agricultural and Forest Meteorology, 218: 204-208.
1085 Meyer, G.E., Neto, J.C., 2008. Verification of color vegetation indices for automated crop
1086 imaging applications. Computers and Electronics in Agriculture 63, 282 - 293.
1087 Mikita, T., Janata, P., Surový, P. 2016. Forest stand inventory based on combined aerial and
1088 terrestrial close-range photogrammetry. Forests, 7(8):165.
1089 Miller, J. 1967. A formula for average foliage density. Australian Journal of Botany 15: 141-
1090 144.
1091 Mokroš, M., Liang, X., Surový, P., Valent, P., Čerňava, J., Chudý, F., Tunák, D., Saloň, Š.,
1092 Merganič, J. 2018. Evaluation of close-range photogrammetry image collection methods for
1093 estimating tree diameters. ISPRS International Journal of Geo-Information, 7(3):93.
1094 Monsi, M., Saeki, T. 1953. The light factor in plant communities and its significance for dry
1095 matter production. Japanese Journal of Botany 14: 22-52.

1096 Nagai, S., Ichie, T., Yoneyama, A., Kobayashi, H., Inoue, T., Ishii, R., Suzuki, R. and Itioka,
1097 T., 2016. Usability of time-lapse digital camera images to detect characteristics of tree
1098 phenology in a tropical rainforest. Ecological informatics, 32: 91-106.
1099 Nagai, S., S. Yoshitake, T. Inoue, R. Suzuki, H. Muraoka, K. N. Nasahara, and T. M. Saitoh.
1100 2014. Year-to-year blooming phenology observation using time-lapse digital camera
1101 images. Journal of Agricultural Meteorology 70:163–170.
1102 Nakaji, T., Oguma, H. and Hiura, T., 2011. Ground-based monitoring of the leaf phenology of
1103 deciduous broad-leaved trees using high resolution NDVI camera images. Journal of
1104 Agricultural Meteorology, 67(2): 65-74.
1105 Nasahara KN, Nagai S (2015) Development of an in-situ observation network for terrestrial
1106 ecological remote sensing -- the Phenological Eyes Network (PEN). Ecological Research,
1107 DOI 10.1007/s11284-014-1239-x
1108 Nilson, T. 1971. A theoretical analysis of the frequency of gaps in plant stands. Agricultural
1109 and Forest Meteorology 8: 25-38.
1110 Noelke, N., Beckschäfer, P. and Kleinn, C., 2015. Thermal canopy photography in forestry-an
1111 alternative to optical cover photography. iForest-Biogeosciences and Forestry, 8(1):1-5.
1112 Nolan, R., Alvarez, L., Padilla-Parra, S., Landini, G. 2019. Autothresholdr. An R Port of the
1113 'ImageJ' Plugin 'Auto Threshold'. URL: https://rorynolan.github.io/autothresholdr/
1114 Osmond, P., 2009. Application of near-infrared hemispherical photography to esti-mate leaf
1115 area index of urban vegetation. In: Seventh International Conference on Urban Climate, 29
1116 June–3 July 2009, Yokohama, Japan.
1117 Otsu, N., 1979. A threshold selection method from gray level his-tograms. IEEE Trans.
1118 Syst. Man Cybern. 9: 62–66.
1119 Paletto, A., Tosi, V. 2009. Forest canopy cover and canopy closure: comparison of assessment
1120 techniques. European Journal of Forest Research, 128(3): 265-272.
1121 Pekin, B., Macfarlane, C. 2009. Measurement of crown cover and leaf area index using digital
1122 cover photography and its application to remote sensing. Remote Sensing, 1(4): 1298-1320.
1123 Peper, P.J., McPherson, E.G. 2003. Evaluation of four methods for estimating leaf area of
1124 isolated trees. Urban Forestry and Urban Greening, 2(1): 19-29.
1125 Phattaralerphong, J., Sathornkich, J., Sinoquet, H. 2006. A photographic gap fraction method
1126 for estimating leaf area of isolated trees: assessment with 3D digitized plants. Tree
1127 physiology 26: 1123-1136.

Piayda, A., Dubbert, M., Werner, C., Correia, A.V., Pereira, J.S., Cuntz, M. 2015. Influence of woody tissue and leaf clumping on vertically resolved leaf area index and angular gap probability estimates. Forest Ecology and Management 340: 103-113.

Pisek, J., Sonnentag, O., Richardson, A.D., Mõttus, M. 2013. Is the spherical leaf inclination angle distribution a valid assumption for temperate and boreal broadleaf tree species? Agricultural and Forest Meteorology 169: 186 - 194.

Qu, Y., Meng, J., Wan, H. and Li, Y., 2016. Preliminary study on integrated wireless smart terminals for leaf area index measurement. Computers and Electronics in Agriculture, 129: 56-65.

R Core Development Team. R: A language and environment for statistical computing. R Foundation for Statistical Computing Vienna (Austria).

Raabe, K., Pisek, J., Sonnentag, O., Annuk, K., 2015. Variations of leaf inclination angle distribution with height over the growing season and light exposure for eight broadleaf tree species. Agricultural and Forest Meteorology 214: 2-11.

Rautiainen, M., Stenberg, P., Nilson, T., 2005. Estimating canopy cover in Scots pine stands. Silva Fennica, 39(1):137-142.

Richardson, A.D., Jenkins, J.P., Braswell, B.H., Hollinger, D.Y., Ollinger, S.V., Smith, M.L., 2007. Use of digital webcam images to track spring green-up in a deciduous broadleaf forest. Oecologia 152(2): 323-334.

Ross, J. 1981. The Radiation Regime and Architecture of Plant Stands. Junk, The Hague: 391.

Ryu, Y., Sonnentag, O., Nilson, T., Vargas, R., Kobayashi, H., Wenk, R., Baldocchi, D.D. 2010. How to quantify tree leaf area index in an open savanna ecosystem: a multi-instrument and multi-model approach. Agricultural and Forest Meteorology 150: 63-76.

Ryu, Y., Verfaillie, J., Macfarlane, C., Kobayashi, H., Sonnentag, O., Vargas, R., Ma, S., Baldocchi, D.D. 2012. Continuous observation of tree leaf area index at ecosystem scale using upward-pointing digital cameras. Remote Sensing of Environment 126: 116-125.

Saitoh, T. M., S. Nagai, J. Yoshino, H. Kondo, I. Tamagawa, and H. Muraoka. 2015. Effects of canopy phenology on deciduous overstory and evergreen understory carbon budgets in a cool-temperate forest ecosystem under ongoing climate change. Ecological Research 30: 267–277.

Salas-Aguilar, V., Sánchez-Sánchez, C., Rojas-García, F., Paz-Pellat, F., Valdez-Lazalde, J.R. and Pinedo-Alvarez, C., 2017. Estimation of vegetation cover using digital photography in a regional survey of central Mexico. Forests, 8(10), p.392.

1161 Schneider, C. A.; Rasband, W. S. & Eliceiri, K. W. 2012. NIH Image to ImageJ: 25 years of
1162 image analysis, Nature methods 9(7): 671-675
1163 Smith, A.M., Ramsay, P.M., 2018. A comparison of ground-based methods for estimating
1164 canopy closure for use in phenology research. Agricultural and Forest Meteorology, 252:
1165 18-26.
1166 Song, W., Mu, X., Yan, G. and Huang, S., 2015. Extracting the green fractional vegetation
1167 cover from digital images using a shadow-resistant algorithm (SHAR-LABFVC). Remote
1168 Sensing, 7(8): 10425-10443.
1169 Sonnentag, O., Hufkens, K., Teshera-Sterne, C., Young, A.M., Friedl, M., Braswell, B.H.,
1170 Milliman, T., O'Keefe, J., Richardson, A.D. 2012. Digital repeat photography for
1171 phenological research in forest ecosystems. Agricultural and Forest Meteorology 152: 159-
1172 177.
1173 Teacher, A.G. F., Griffiths D.J., Hodgson D.J., Inger R. 2013. Smartphones in ecology and
1174 evolution: a guide for the app-rehensive. Ecology and Evolution 3: 5268-5278.
1175 The GIMP team, GIMP 2.10, 2018.
1176 Toda, M., Nakai, T., Kodama, Y., Hara, T. 2018. Using digital cover photography to track the
1177 canopy recovery process following a typhoon disturbance in a cool–temperate deciduous
1178 forest. Canadian Journal of Forest Research 48(999): 1-9.
1179 Van Elsacker, P., Keppens, H. and Impens, I., 1983. A simple photographical method for
1180 analyzing the radiation interception by an individual tree. Agricultural Meteorology, 29(4):
1181 285-298.
1182 Van Gardingen PR, Jackson GE, Hernandez- Daumas S, Russell G, Sharp L 1999. Leaf area
1183 index estimates obtained for clumped canopies using hemispherical photography.
1184 Agricultural and Forest Meteorology 94 : 243-257.
1185 Wagner S, Hagemeier M 2006. Method of segmentation affects leaf inclination angle
1186 estimation in hemispherical photography. Agric. For. Meteor. 193: 12-24.
1187 Wang WM, Li ZL, Su HB 2007. Comparison of leaf angle distribution functions: effects on
1188 extinction coefficient and fraction of sunlit foliage. Agricultural and Forest Meteorology
1189 143: 106 - 122.
1190 Wang YS, Miller DR (1987). Calibration of the hemispherical photographic technique to
1191 measure leaf area index distributions in hardwood forests. Forest Science 33: 110-126.
1192 Warren-Wilson 1960. Inclined point quadrats. New Phytol. 59: 1-7.

1193 Weiss M, Baret F, Smith GJ, et al 2004. Review of methods for in situ leaf area index (LAI)
1194 determination Part II. Estimation of LAI, errors and sampling. Agric For Meteorol 121:37–
1195 53. doi: 10.1016/j.agrformet.2003.08.001
1196 Welles, J.M., Norman, J.M. 1991. Instrument for indirect measurement of canopy architecture.
1197 Agric. J. 83: 818–825.
1198 Westoby, M.J., Brasington, J., Glasser, N.F., Hambrey, M.J. and Reynolds, J.M. 2012.
1199 'Structure-from-Motion' photogrammetry: A low-cost, effective tool for geoscience
1200 applications. Geomorphology, 179: 300-314.
1201 Yan G, Hu R, Luo J, Weiss M, Jiang H, Mu X, Xie D, Zhang W 2019. Review of indirect
1202 optical measurements of leaf area index: Recent advances, challenges, and perspectives.
1203 Agricultural and Forest Meteorology, 265: 390-411.
1204 Zhang Y, Chen JM, Miller JR 2005. Determining digital hemispherical photograph exposure
1205 for leaf area index estimation. Agricultural and Forest Meteorology 133: 166–181.
1206 Zou J, Yan G, Zhu L, Zhang W 2009. Woody-to-total area ratio determination with a
1207 multispectral canopy imager. Tree Physiol. 29 (8), 1069–1080
1208
1209

Table captions

Table 1. Clumping correction formulae available from literature.

Reference	Type	Formula
Lang and Xiang (1986)	Gap fraction distribution	$\Omega_{LX}(\theta) = \frac{-\ln\left(\frac{1}{n}\sum_{i=1}^{n} P_i(\theta)\right)}{\frac{1}{n}\left(-\sum_{i=1}^{n} \ln P_i(\theta)\right)}$
Chen and Cihlar (1995)	Gap size distribution	$\Omega_{CC}(\theta) = \frac{\ln\left(F_m(0,\theta)\right)}{\ln\left(F_{mr}(0,\theta)\right)}\left[1 + \frac{F_m(0,\theta) - F_{mr}(0,\theta)}{1 - F_m(0,\theta)}\right]$
Leblanc (2002)	Combined gap fraction and size distribution	$\Omega_{CLX}(\theta) = \frac{n\, ln\overline{P(\theta)}}{\sum_{k=1}^{n} ln[P_k(\theta)]/\Omega_{CC_k}(\theta)}$
Chianucci et al. (2019)	Combined gap fraction and size distribution	$\Omega_{LXG}(\theta) = \frac{-ln\left(\sum_{i=1}^{n} w_i' P_{i\downarrow}(\theta)\right)}{-ln\left(\sum_{i=1}^{n} w_i' P_{i\uparrow}(\theta)\right)}$

Abbreviations: n is the number of azimuth segments (for DHP); F_m is the total gap fraction, F_{mr} is the gap fraction after removing large gaps; k is the considered azimuth segment (for DHP); w_i are non-increasing weights for decreasingly-ordered ($P_{i\downarrow}$) and increasingly-ordered ($P_{i\uparrow}$) gap fraction

1218 **Table 2.** Summary statistics of the six leaf inclination angle distribution types as calculated
1219 by Goel and Strebel (1984).
1220

Leaf inclination angle distribution type	Mean (°)	μ	ν
Planophile	26.8	2.770	1.172
Erectophile	63.2	1.172	2.770
Plagiophile	45.0	3.326	3.326
Extremophile	45.0	0.433	0.433
Uniform	45.0	1.000	1.000
Spherical	57.3	1.101	1.930

1221
1222

1223 **Table 3.** Comparison between LAI-2200 and DHP features
1224

Feature	**LAI-2200**	**DHP**
Simplicity of usage	Yes	No
Cost-effectiveness	No	Yes
Require Above readings	Yes	No
Calculate clumping index	Partly	Yes
Use in direct sky conditions	Yes	No
Visual quality check	No	Yes
Comparability between operators	Easy	Difficult
Possibility to set number and size of zenith rings	No	Yes
Possibility to set number of azimuth segments	No	Yes

1225
1226

1227 **Table 4.** Comparison of different softwares for DHP image analysis.
1228

Software	Pixel classification	Availability	Clumping index
Winscanopy	Automatic and interactive (manual); color classification	Commercial	Yes
GLA	Manual	Free	No
CAN-EYE	Automatic and interactive (manual); color classification	Free	Yes
HemiView	Manual	Commercial	No
Hemisfer	Automatic and interactive (manual)	Commercial or Institutional[1]	Yes
CIMES	Automatic and interactive (manual)	Free	Yes

1229 [1] Hemisfer has bot commercial and institutional (non-profit) license.
1230

Table 5. TLS scanner parameters used in the sampled beech plots. Resolution refers to the ratio of the maximum resolution of 40,000 pts/360° for each rotation of the scan head. Noise compression factor 1× indicates no resampling.

TLS instrument model	FARO Focus 3D X130
Scan density	976 kpt s^{-1}
Angular resolution	0.009°
Beam divergence	0.19 mrad
FOV (H,V)	360°, 150°
Wavelength	1550 nm
Resolution	1/1
Noise compression	1x

1239 **Table 6.** Parameters setup for the three canopy photographic techniques tested in the case
1240 study
1241

Parameters	DHP	DCP	57°
Camera	Nikon D90		
Lens	Sigma 4.5 mm	AF Nikkor 50 mm	Sigma 4.5 mm
Image resolution (pixels)	4288x2848		
Image pixels used to sample the canopy (%)	~24%	100%	~3% (~14% of DHP image area)
Image format	NEF		
Mode	Aperture-priority		
ISO	200		
F-value	10		
Exposure metering	Center-weighted	Matrix	Center-weighted
Relative exposure value (REV; number of stops)	-1		
Number of images	9	45	9
Image thresholding method	Two-corner method (Macfarlane 2011)		
Zenith angle range used for analysis	0°-75°	0°-15°	52°-62°
Zenith angle bins (number x size)	5 x 15°	1 x 15°	1 x 10°
Extinction coefficient	Derived from gap inversion	Independently measured	*A-priori* known

1242
1243

Figure captions

Figure 1. (Left): Leaf inclination angle distribution functions. (Right): G-function

Figure 2. (Left): An example of a digital hemispherical image of a broadleaf forest. (Right): the fisheye-lens sensor of LAI-2200 Plant Canopy Analyzer (Image courtesy of LI-COR Biosciences).

Figure 3. An example of a cover image that has been classified into canopy (green), small within-crown gaps (white) and large between-crowns gaps (yellow). Crown cover is the fractional cover of green and white pixels, foliage cover is the fractional cover of green pixels, and crown porosity is the ratio of white to green and white pixels.

Figure 4. An example of a 57° image

Figure 5. An example of a suitable leaf for leaf inclination angle measurements from levelled photography.

Figure 6. An example of a full-frame hemispherical image. All the image pixels are used in full-frame hemispherical images, increasing the number of pixels used for canopy analysis compared to circular hemispherical photography.

Figure 7. Example of an intensity image derived from raw TLS scan data.

Figure 8. (Left): Sampling protocol used for acquiring DCP (crosses) and DHP (squares) images in each 50 m x 50 m beech plot. TLS measurements were also performed in the same points of DHP (squares). (Right): histogram of a well-exposed DHP image obtained after contrast-stretch and raw-to-jpeg conversion.

Figure 9. Difference between gap fraction estimates obtained from DCP and DHP at 0°-15° zenith range (y-axis) against foliage cover (i.e, the complement of total gap fraction) estimated from DCP (x-axis).

Figure 10. Comparison with effective PAI estimates obtained from overstory (DCP, DHP and 57°) photography (y-axis) against reference values measured from terrestrial laser scanning (x-axis).

1271 **Figure 11**. Example of the LAB2 classification proposed by Macfarlane and Ogden (2012).
1272 The procedure combines a green vegetation index (GLA=(2G-R-B)/(2G+R+B)) and the
1273 a* and b*channels from a CIELAB colour space conversion to get an estimate of
1274 understory cover. For details, see Macfarlane and Ogden (2012).

1275 **Figure 12.** (Left): An example of an individual urban tree crown photographed using DCP.
1276 (Right): Green vegetation has been selected using a vegetation index (GEI=2G-R-B).

Annex 1: Nomenclature

Symbol	Description
FOV	Field of view
FHP	Film hemispherical photography
DHP	Digital hemispherical photography
DCP	Digital cover photography
LP	Leveled photography
57°	Fifty-seven degree photography
RVP	Restricted view photography
LAI	Leaf area index (omitting the contribution of WAI)
LAI_e	Effective leaf area index (not considering clumping correction)
WAI	Woody area index
PAI	Plant area index (including WAI contribution)
PAI_e	Effective PAI (not considering clumping correction)
θ	Zenith angle
$P(\theta)$	Gap fraction at the zenith angle θ
P_0	Gap fraction close to the zenith (0°-15° zenith angle range)
P_1	Gap fraction centered at 1 radian (52°-62° zenith angle range)
$G(\theta)$	Foliage projection coefficient at the zenith angle θ
$k(\theta)$	Extinction coefficient at the zenith angle θ
k	Extinction coefficient at the zenith
θ_L	Leaf inclination angle
$f(\theta_L)$	Leaf inclination angle distribution function
$\Omega(\theta)$	Clumping index at the zenith angle θ
Ω	Clumping index calculated as the ratio of LAIe to true (clumping corrected) LAI
CCO	Crown cover
FCO	Foliage cover
CP	Crown porosity
CCL	Canopy closure
Ω_0	Clumping index estimated from DCP
Ω_{LX}	Clumping index from Lang and Xiang (1986) method
Ω_{CC}	Clumping index from Chen and Cihlar (1995) method
Ω_{CLX}	Combined gap fraction and gap size clumping index from Leblanc (2002)
Ω_{LXG}	Clumping index from Chianucci et al. (2019)
Ω_{APP}	Apparent clumping index calculated by LAI-2200
UAV	Unmanned aerial vehicle

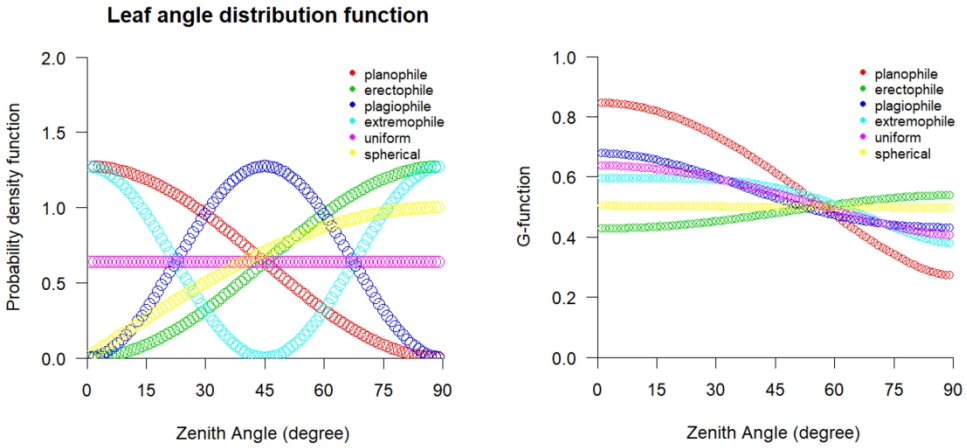

Figure 1. (Left): Leaf inclination angle distribution functions. (Right): G-function

282x149mm (300 x 300 DPI)

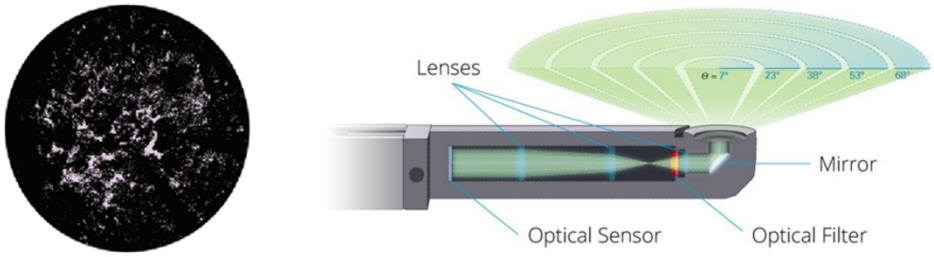

Figure 2. (Left): An example of a digital hemispherical image of a broadleaf forest. (Right): the fisheye-lens sensor of LAI-2200 Plant Canopy Analyzer (Image courtesy of LI-COR Biosciences).

189x60mm (300 x 300 DPI)

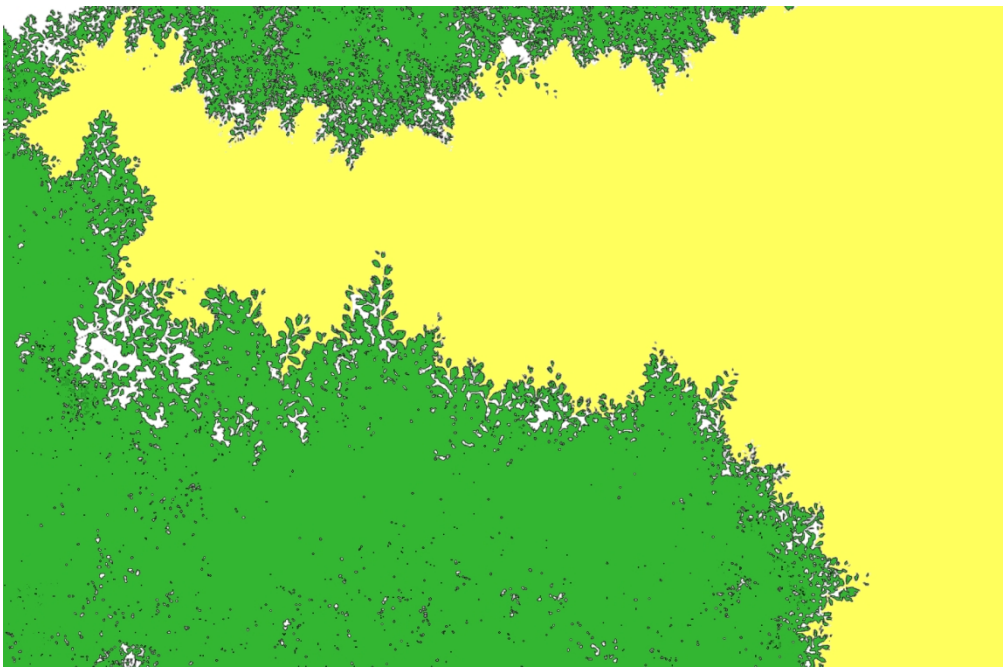

Figure 3. An example of a cover image that has been classified into canopy (green), small within-crown gaps (white) and large between-crowns gaps (yellow). Crown cover is the fractional cover of green and white pixels, foliage cover is the fractional cover of green pixels, and crown porosity is the ratio of white to green and white pixels.

140x92mm (300 x 300 DPI)

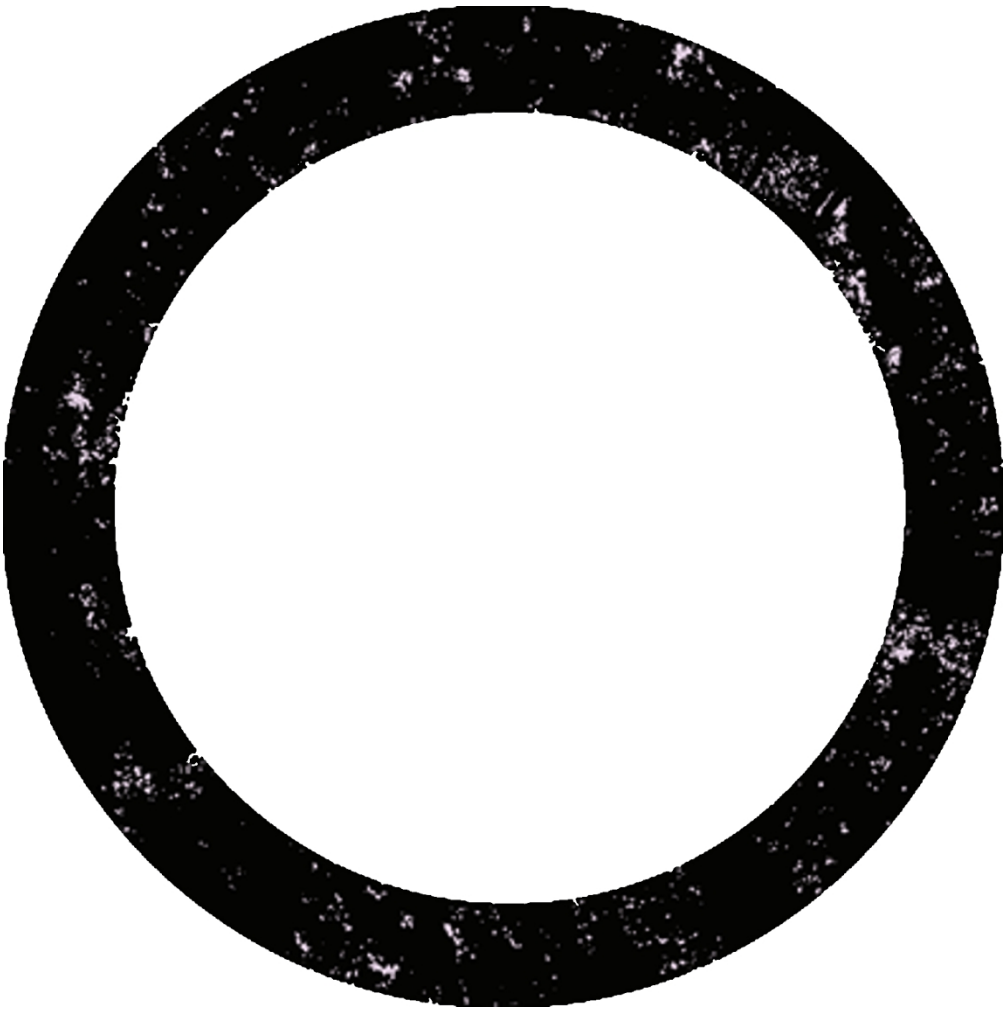

Figure 4. An example of a 57° image

140x140mm (300 x 300 DPI)

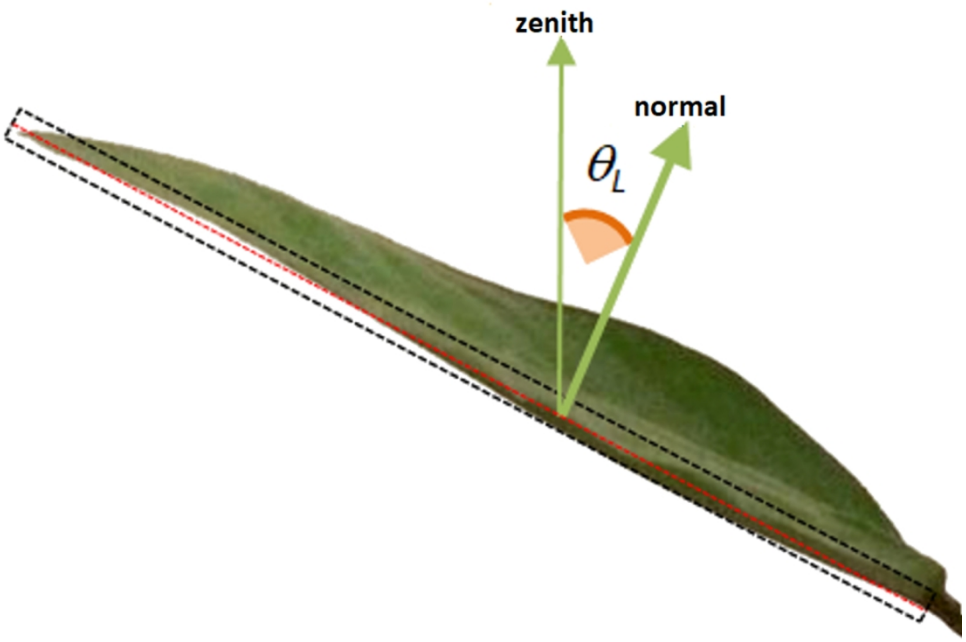

Figure 5. An example of a suitable leaf for leaf inclination angle measurements from levelled photography.

140x106mm (300 x 300 DPI)

Figure 6. An example of a full-frame hemispherical image. All the image pixels are used in full-frame hemispherical images, increasing the number of pixels used for canopy analysis compared to circular hemispherical photography.

189x126mm (300 x 300 DPI)

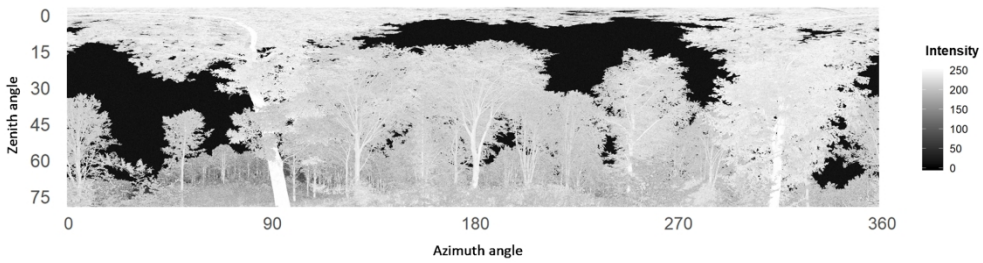

Figure 7. Example of an intensity image derived from raw TLS scan data.

189x51mm (300 x 300 DPI)

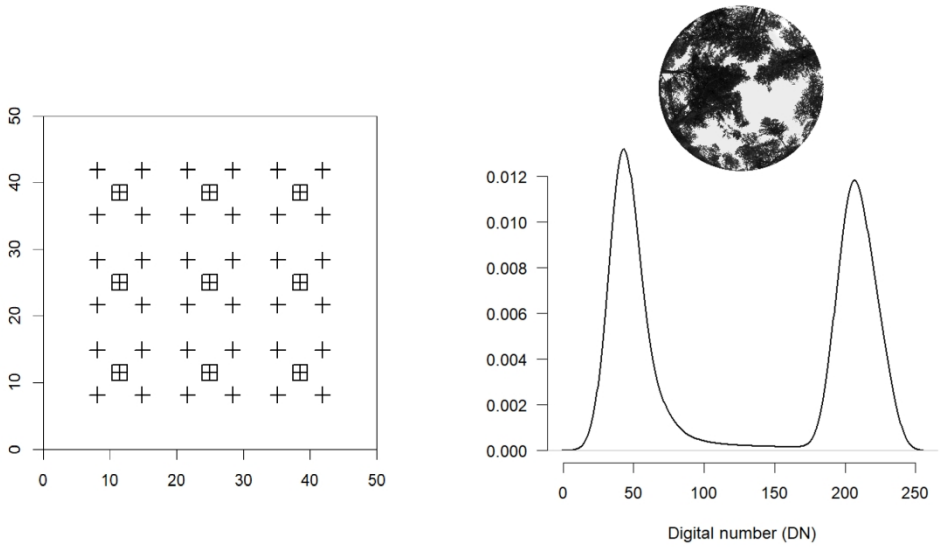

Figure 8. (Left): Sampling protocol used for acquiring DCP (crosses) and DHP (squares) images in each 50 m x 50 m beech plot. TLS measurements were also performed in the same points of DHP (squares). (Right): histogram of a well-exposed DHP image obtained after contrast-stretch and raw-to-jpeg conversion.

189x111mm (300 x 300 DPI)

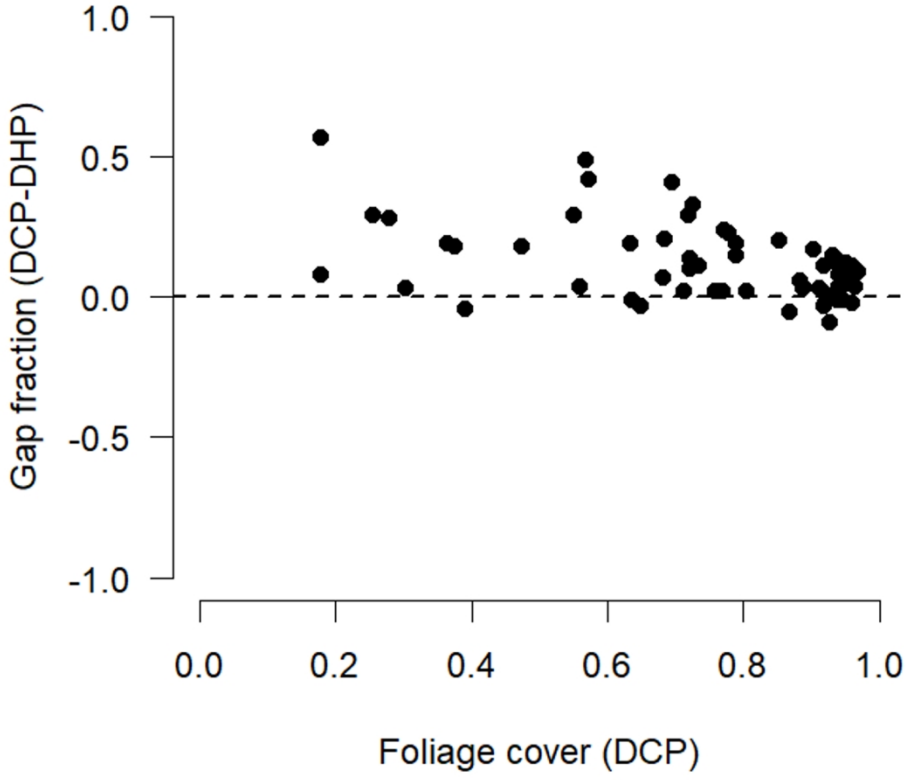

Figure 9. Difference between gap fraction estimates obtained from DCP and DHP at 0°-15° zenith range (y-axis) against foliage cover (i.e, the complement of total gap fraction) estimated from DCP (x-axis).

140x140mm (300 x 300 DPI)

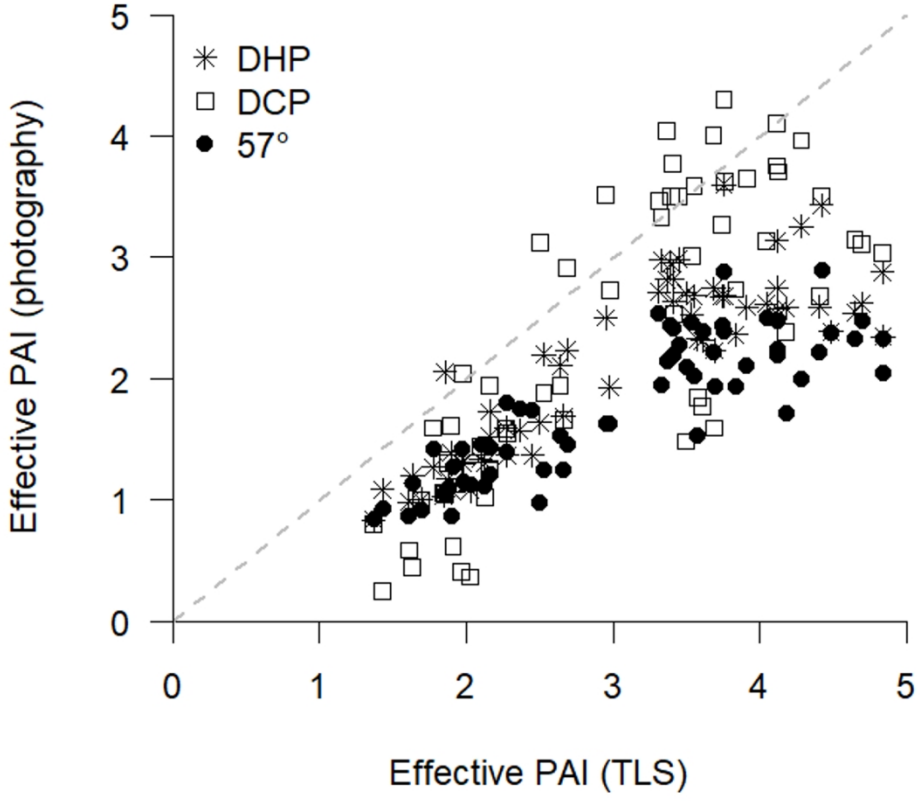

Figure 10. Comparison with effective PAI estimates obtained from overstory (DCP, DHP and 57°) photography (y-axis) against reference values measured from terrestrial laser scanning (x-axis).

140x140mm (300 x 300 DPI)

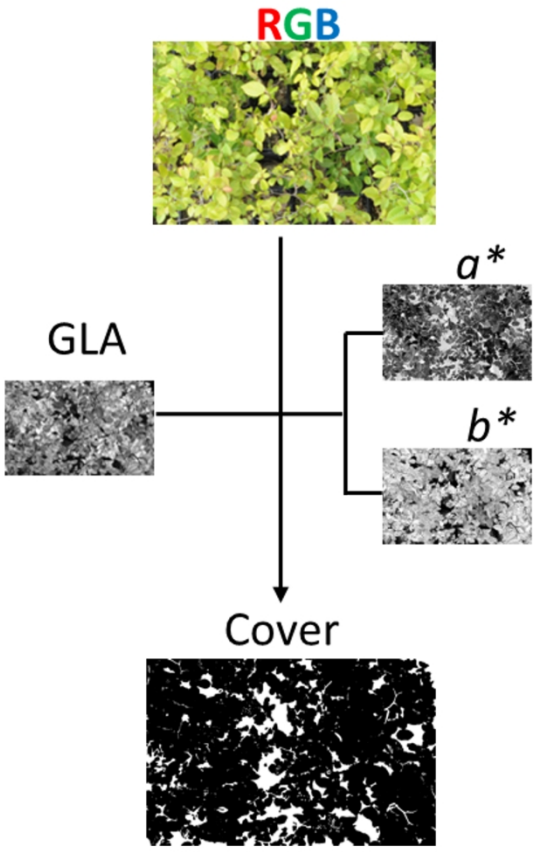

Figure 11. Example of the LAB2 classification proposed by Macfarlane and Ogden (2012). The procedure combines a green vegetation index (GLA=(2G-R-B)/(2G+R+B)) and the a* and b*channels from a CIELAB colour space conversion to get an estimate of understory cover. For details, see Macfarlane and Ogden (2012).

140x211mm (300 x 300 DPI)

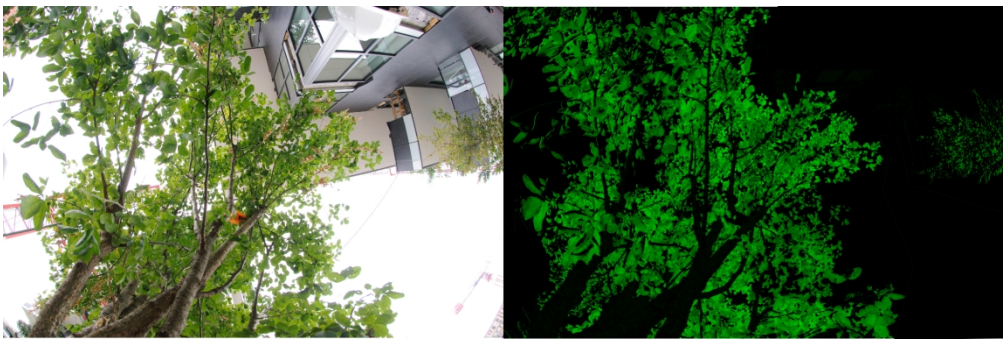

Figure 12. (Left): An example of an individual urban tree crown photographed using DCP. (Right): Green vegetation has been selected using a vegetation index (GEI=2G-R-B).

189x63mm (300 x 300 DPI)